

“© 2018 IEEE. Personal use of this material is permitted. Permission from IEEE must be obtained for all other uses, in any current or future media, including reprinting/republishing this material for advertising or promotional purposes, creating new collective works, for resale or redistribution to servers or lists, or reuse of any copyrighted component of this work in other works.”

Development of a Fuzzy-Logic-Based Energy Management System for a Multi-Port Multi-Operation Mode Residential Smart Micro-grid

Mohammad Jafari*, *Member, IEEE*, Zahra Malekjamshidi, *Student Member, IEEE*, Dylan Du Lu, *Senior Member, IEEE*, and Jianguo Zhu, *Senior Member, IEEE*

Abstract—In this paper a grid-tied residential smart micro-grid topology is proposed which integrates energies of a PV, a fuel cell and a battery bank to supply the local loads through a combination of electric and magnetic buses. In contrast to multiple-converter based micro-grids with a common electric bus, using a multi-port converter with a common magnetic bus can effectively reduce the number of voltage conversion stages, size and cost of the renewable energy system and isolates the conversion ports. The resultant topology utilizes a centralized system level control which leads to the faster and more flexible energy management. The proposed micro-grid is able to operate in multiple grid-connected and off-grid operation modes. A fuzzy controlled energy management unit (EMU) is designed to select the appropriate operation mode considering both real-time and long-term-predicted data of the energy generation and consumption. A mode transition process is designed to smooth the mode variation by using a state transition diagram and bridging modes. To improve the micro-grid operation performance, appropriate control techniques such as synchronized bus-voltage balance are used. A prototype of the proposed micro-grid and the EMU are developed and experimentally tested for three different energy management scenarios. Energy distribution and energy cost analysis are performed for each scenario to validate the proposed control method.

Index Terms—Energy management, fuzzy logic control, multi-port dc-dc converter, renewable energy system, residential micro-grid

I. INTRODUCTION

OVER the last decade, there has been a great interest in renewable energy sources as a feasible solution to mitigate environmental issues and reduce the dependence on the traditional sources for electricity generation. The need for technology for integrating these non-traditional types of energy sources into the existing grid has motivated the development of the new smart micro-grid concept. The smart micro-grid is recognized as a feasible solution to the new challenges of existing grid network such as increasing energy demand and penetration of renewable energy sources at the consumer end [1]-[3]. On the other hand, the electricity market share in the residential sector has increased substantially with an average annual growth rate of 9.4% from 1960 to 1973 and a slower rate of 2.7%

Manuscript received December 11, 2017; revised April 18, 2018; accepted June 11, 2018.

M. Jafari, Z. Malekjamshidi, and D.Lu are with the School of Electrical and Data Engineering, University of Technology Sydney, NSW, Australia. e-mail:(mohammad.jafari@uts.edu.au; z.malekjamshidi@student.uts.edu.au; Dylan.Lu@uts.edu.au)

Jianguo Zhu is with the School of Electrical and Information Engineering, The University of Sydney, NSW, Australia. (e-mail: Jianguo.zhu@sydney.edu.au)

from 1973 to 2010 [4]. Therefore, design and development of residential based renewable energy systems have attracted great interest over the past decades. In Australia, solar PV systems continue to be very popular in the residential sector and about 1.5 million Australian homes are now using solar panels [5]. The proportion of solar energy users is about 18 % and in some urban areas reaches over 50 % [6].

In the residential micro-grids, energy control boxes have been traditionally used to control the energy consumption inside the households by automatic control of some shiftable loads [7]. This enables the residential consumers to adapt their energy consumption to the time-pricing and new services of the main grid [8]. On the other hand, using energy control boxes has improved the power efficiency and quality in the main grid by shifting loads to the off-peak hours [8], [9]. Recent energy management systems are designed to match the generated energy of renewables inside the micro-grid with the load demand in an optimal way with minimum customer intervention [10], [11]. They can control the household smart appliances through a local network [12], [13] and communicate with the regional smart grid control centre by using a higher level communication networks (cellular networks and 4G technologies such as WiMAX) to adapt their operation with the requirements [14],[15]. Different methods of optimal energy management and control in residential renewable energy systems have been described in the literature [16]-[18]. The energy management objectives have been selected as minimizing the micro-grid operation cost [19], [20], maximizing the revenue due to the electricity market price [21], minimizing micro-grid operation effect on the main grid [22], improving power quality [23], safety and reliability [24]. In this regard, a wide range of research on energy management systems considering different methods, micro-grid structures, scenarios and objectives have been conducted [25],[26].

Fuzzy controllers have been successfully used as supervisory control and energy management unit (EMU) in various hybrid renewable energy systems [27]-[32]. In particular, they have been used as load frequency controller in microgrids [27], supervisory control in electric vehicles for energy management [28],[29], and power split [31]. Nevertheless, their application as household energy management system is not widely studied. In [32] a multi-agent fuzzy logic based energy management is introduced to manage the energy in a stand-alone renewable energy system. In [30] a fuzzy based EMU is used in a residential micro-grid to minimize the grid power fluctuations taking into account the battery state of charge (SOC).

From the topological point of view, the majority of proposed residential micro-grid topologies utilize multiple conversion units and common dc or ac electrical bus [30],

[33]. In contrast, using a magnetic bus in small-scale applications such as residential micro-grids presents considerable advantages [34]-[36]. It can reduce the number of voltage conversion blocks and system size and the control complexity by using a centralised controller, eliminate the voltage and frequency instability problems, and provide isolation between the micro-grid elements [37]-[39].

In this paper, a residential smart micro-grid topology is introduced based on a common magnetic bus. The resultant flexibility in power flow direction and control of the proposed micro-grid leads to a large number of operation modes (16 grid-connected and 8 off-grid operation modes) and more efficient energy management. A fuzzy logic based EMU is designed to define the appropriate operation mode of the micro-grid due to its simplicity and independence to the intrinsic nonlinearities of the micro-grid components.

In contrast to the deterministic rule-based energy management systems, the fuzzy controllers are simple, robust and independent of intrinsic nonlinearities of the micro-grid components [28], [30], [40]. They do not need complex mathematical modelling which normally used in classic controllers and help to build a comprehensive and intuitive energy management strategy based on the simple linguistic rules which can effectively simplify the energy management process in the case of a large number of system statuses and operation modes [41].

In the proposed micro-grid system, the reference signals of the converter controllers and the system's operation mode need to be adjusted continuously according to the real-time variations of the input variables. Therefore, using rule-based control methods increases the complexity due to the large number of operation modes, large number of input variables and their non-linear nature. While, in the case of using fuzzy controllers, only the main rules and selected operation modes can be grasped which simplify the control process [42]. Furthermore, the common optimisation-based energy management methods using linear programming, dynamic programming and quadratic programming techniques result in extensive computational efforts and require relaxation techniques due to the presence of nonlinear and integer variables and large number of operation modes.

The main contributions of this paper can be summarised as:

Besides introducing an interesting topology of residential micro-grid based on a common magnetic bus, several control techniques are employed to improve the micro-grid performance according to the required standards for grid-connected residential renewable energy systems (AS/NZS4777, IEEE1547 and IEC61727) [43],[44] including:

- An interleaved topology is introduced in the PV port, which can reduce the high-frequency current ripple and result in a more stable MPPT process, smaller filter components and wider input voltage range;
- A synchronized dc bus voltage balance (SBVB) technique is proposed for the TAB converter ports to reduce the root-mean-square (RMS) and peak currents in the windings of the magnetic link and also increase the soft switching operation range. It can increase the entire micro-grid efficiency as validated by experimental tests;

- A feed-forward compensation block is introduced in the inverter control loop to reduce the low frequency (2ω) ripple propagated from the inverter output on high voltage dc bus and further on fuel cell and PV buses, which can improve the MPPT performance.

In the system level control, the proposed micro-grid is able to operate in a large number of different grid-connected and islanded modes (20 different modes in total) compared to the systems previously reported in the literature. Three different energy management scenarios are studied in detail, and the energy distribution and energy cost analysis are provided for each scenario.

- A novel fuzzy logic-based energy management including the short-term and long-term controllers is proposed for the micro-grid. Therefore, both the real-time condition and long-term predictions of energy generation and consumption have been taken into account.
- Hysteresis based membership functions for the output variables of the fuzzy controller are introduced to reduce the undesirable oscillations between the operation modes.
- A novel mode transition strategy is designed to smooth the mode transition by defining the bridging modes, mode transition flowchart and a state transition diagram (STD).

This paper mainly focused on the micro-grid system-level control and energy management although a brief review of the device-level control system is provided in the next section.

II. STRUCTURE OF THE PROPOSED MICRO-GRID AND CONTROL TECHNIQUES

The electrical schematic of the proposed micro-grid and controllers are presented in Fig.1. The value of micro-grid components and parameters are presented in Table.III, Appendix. As can be seen, the micro-grid includes three H-bridge ports (ports one, two and three) connected to a multi-winding transformer to form a triple active bridge (TAB) dc-dc converter. The multi-winding transformer provides a high-frequency magnetic bus for distribution of power among the ports in the form of magnetic flux. The dc bus voltages V_{b1} , V_{b2} and V_{b3} are converted to high-frequency ac square waves by using H-bridge converters of port one, two and three respectively. The dc high voltage on port one, V_{b1} (280-320 V) is converted to a low frequency (50 Hz) ac voltage by using a single phase bidirectional inverter. The inverter can be used reversely as a rectifier to supply the grid energy into the high voltage dc bus and is further used to charge the battery by activating ports two and four simultaneously. The fuel cell stack is connected to the port two via a low voltage bus (50-70 V). A bi-directional buck-boost converter presented as port four links the battery to the dc bus. It operates in buck mode to charge the 24 V battery bank and in boost mode to discharge the battery into the bus. The PV power is transferred to the capacitor C_3 by using interleaved boost converter and further to the magnetic bus by using shared switching devices S_{31} - S_{34} in port three. An electrolyzer is assumed to be used as a local load to generate the required hydrogen for the fuel cell. As illustrated in Fig.1, the proposed micro-grid is controlled in device level by two digital signal processors (DSPs) including DSP1 for dc-dc converters and DSP2 for the single-phase inverter. On the other hand, a personal computer (PC) is used as system level controller and performs the operation mode control

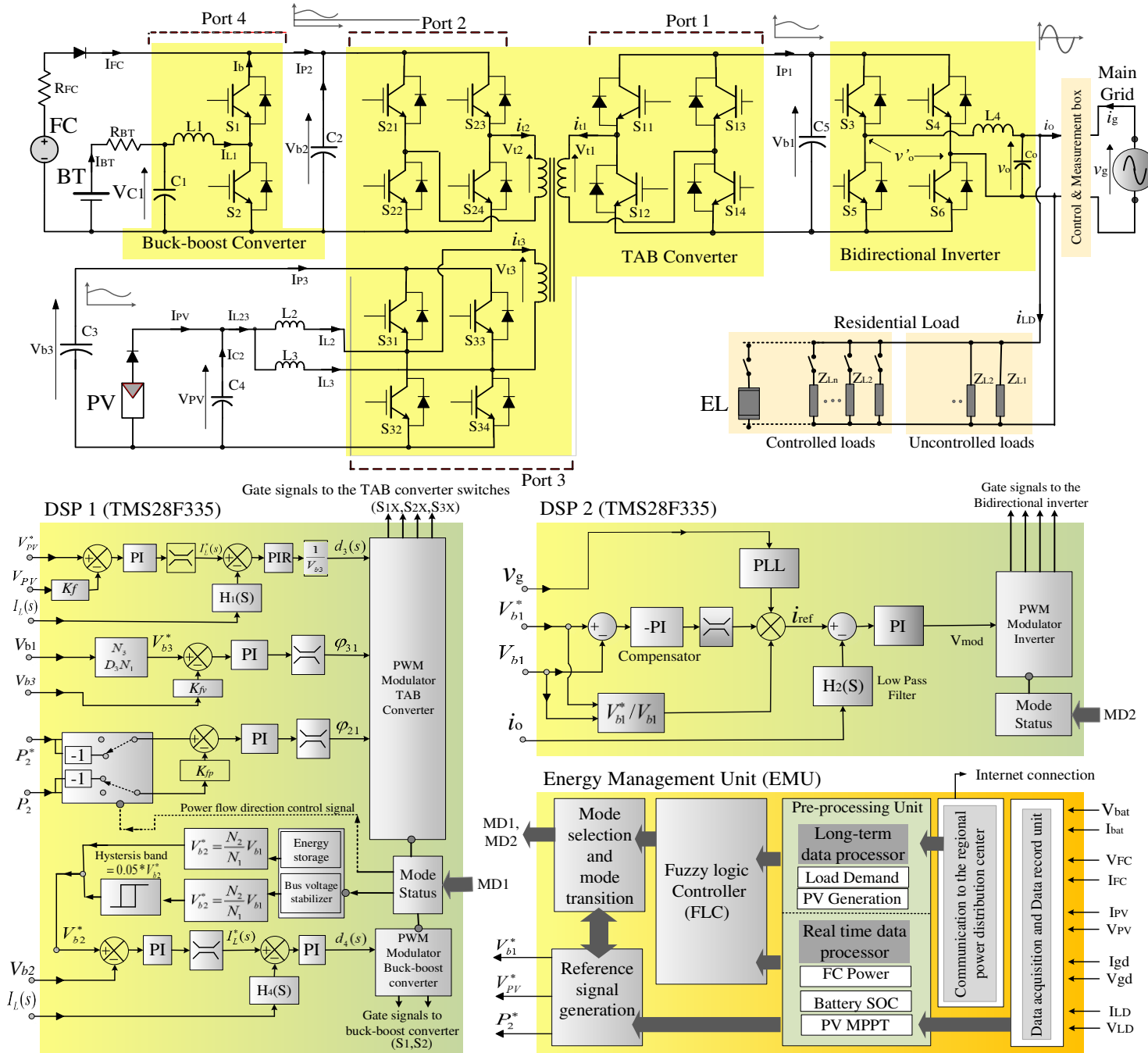


Fig.1. Structure of the proposed micro-grid including device level controllers and energy management unit

and energy management. The proposed micro-grid can operate in several modes according to the power flow direction and active sources and loads. The operation mode control signals (MD1 and MD2) are generated by mode selection and transition unit and sent to the PWM generators in DSP1 and DSP2. The direction and amount of power flow in the magnetic bus are controlled by introducing phase shift angles φ_{21} and φ_{31} between ports two and three to port one respectively. As can be seen in Fig.1, the phase shift φ_{21} is used to control the power flow from port two to one (P₂₁) according to the reference signal provided by EMU and φ_{31} is used to control the power transferred from port three (PV port) to port one by regulating bus voltage, V_{b3} . The power flow and voltage regulation control systems and the magnitude and phase bode diagrams are presented in Fig.2. As can be seen, the phase shift angles φ_{31} and φ_{21} are controlled by single loop proportional-integral (PI) controllers. To decouple the power flow control and voltage

regulation loops, the compensators are designed to provide a slower dynamic response for power flow control loop compared with that of voltage regulation.

In the battery port, the bidirectional buck-boost converter is controlled by conventional dual loop controller as presented in Fig.3. The outer voltage control loop generates a reference signal for the inner current control loop which presents higher dynamic response. The generated reference signal depends on the battery application as energy storage or as a bus-voltage regulator. In the first case, the reference signal (V_{b2}^*) is following V_{b1} variations due to the SBVB technique requirement to guarantee zero voltage switching (ZVS) operation of the converter ports by applying equal volt-second on all windings of the magnetic link. In the second case, the reference voltage (V_{b2}^*) is generated similarly although, a 5% hysteresis band with maximum and minimum bus voltage is considered.

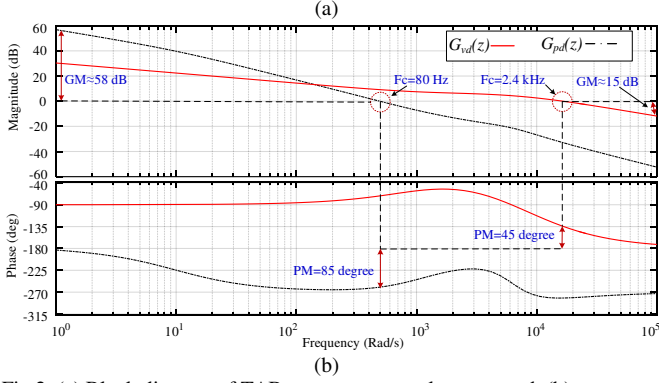
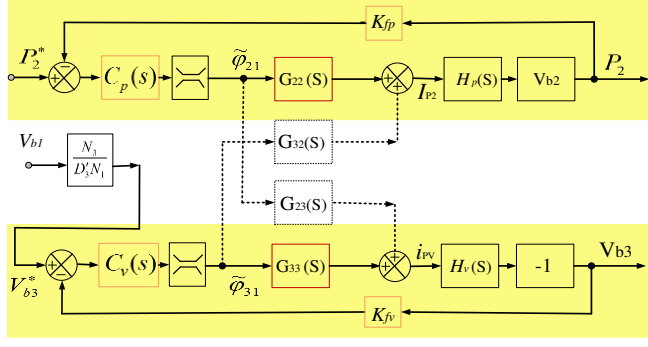


Fig.2. (a) Block diagram of TAB converter control system and, (b) magnitude and phase bode diagram of the TAB converter

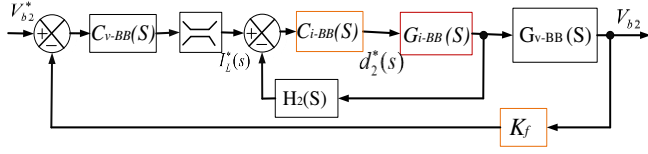


Fig.3. The control diagram of the bidirectional buck-boost converter

In the PV port C_3 is used as an energy buffer between the interleaved boost converter and H-bridge dc-ac converter. Therefore, the PV voltage control loop (for MPPT) by using duty ratio (d_3), operates independently of the bus-voltage control by using phase shift angle (φ_{31}). To maintain the MPPT, a dual loop proportional-integral-resonant (PIR) compensator is designed [45]. The closed-loop control system and the magnitude and phase bode diagrams are presented in Fig.4. The duty ratio of driving signal of S_{32} and S_{34} (d_3) is controlled to adjust the PV output voltage (V_{PV}) on a reference signal (V_{PV}^*) to maintain the MPPT. The reference signal is generated by EMU according to a variable step size incremental conductance (INC) method [46]. The resonant compensator is added to the current control loop to reduce the 2ω low-frequency ripple propagated from the high-voltage dc bus (V_{b1}) linked to the inverter [45]. The transfer functions of the PI controllers can be written in the general form as

$$C(S) = K_p + \frac{K_I}{S} \quad (1)$$

where K_p and K_I are the proportional and integral coefficients respectively and are defined by using the required crossover frequency (ω_c) and the phase margin (φ_m) of the voltage and current control loops from

$$K_p = \frac{-\omega_c \sin(\theta)}{|G(j\omega_c)|}, \quad K_I = \frac{\cos(\theta)}{|G(j\omega_c)|} \quad (2)$$

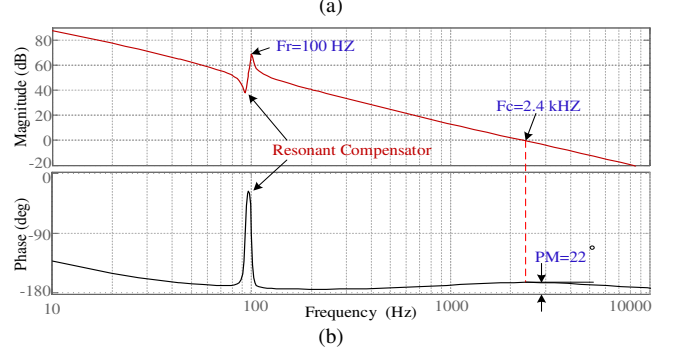
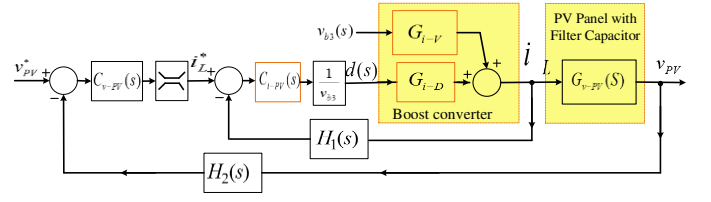


Fig.4. (a) The control diagram and (b) the bode diagram of the interleaved boost converter

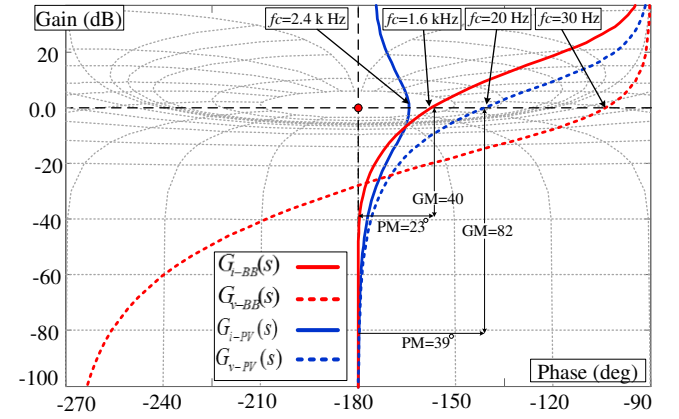


Fig.5. The Nichols chart of phase and gain variation of the buck-boost bi-directional and the interleaved boost converter voltage and current control loops.

where $\theta = 180 + \varphi_m - \angle G(j\omega_c)$, and $G(j\omega_c)$ is the open loop transfer function of the outer voltage or inner current control loops [47]-[49]. The Nichols chart presented in Fig.5 shows the voltage and current control open-loop transfer functions of the bidirectional buck-boost (G_{v-BB} , G_{i-BB}) and interleaved boost (G_{v-PV} , G_{i-PV}) converters. The crossing frequencies, phase margin and gain margins show the stability of designed controllers. The pole-zero locus of the transfer functions of the voltage control loop for the buck-boost and interleaved converters are presented in Fig.6. As can be seen, the system poles are varying in the left half plane of the real-imaginary map for entire variation range of the input voltage and load power. The load power variation represents the change in the duty cycle and minimum input voltage results in the maximum duty cycle. This confirms that the system is always stable in the designed operating range.

The state averaged equations and the resultant transfer functions and other control blocks of the dc-dc converters are presented in the Appendix. The dc voltage on port one (V_{b1}) is selected as a reference for other two ports and therefore should be kept constant in all operation modes on the reference value provided by EMU. It is regulated by bidirectional inverter using inverter/rectifier operation modes. As presented in Fig.7, a dual loop control system

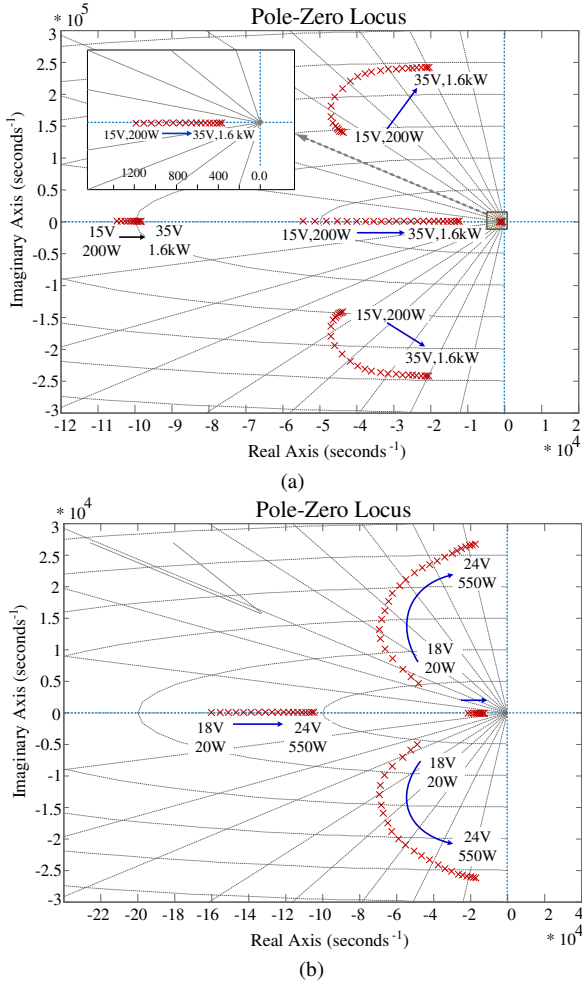


Fig.6. Pole-zero locus of the transfer functions of voltage control loop, (a) buck-boost converter, and, (b) interleaved boost converter

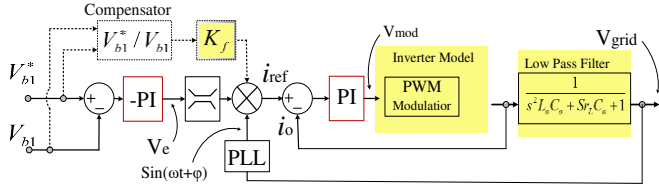


Fig.7. The control scheme of bi-directional single phase inverter

with PI compensators in voltage and current control loops is designed for the bidirectional inverter. A direct-current control technique is applied to the bidirectional inverter to force the inverter current to follow the grid voltage [50]. This is due to the current standards of power factor requirement for grid-connected residential micro-grids [43]. A feed-forward compensation block (V_{b1}^*/V_{b1}) applies a reverse fluctuating signal with the frequency (2ω) to the output current reference signal to cancel the low-frequency ripple propagated from inverter output on the high-voltage dc bus [50]. More details on the system waveforms, controller design and the micro-grid dynamic response will be provided in the future publications and this paper is mainly focused on the energy management technique.

III. ENERGY MANAGEMENT UNIT

Three levels of control with different time steps are designed for decision making and management of the proposed micro-grid. At the highest level, the regional

distribution network control centre manages the total power flow and power quality of the distribution network and communicates with the EMU in each residential micro-grid. In system level, the EMU manages the energy inside the residential micro-grid and selects the operation modes. In the device level, DSPs (DSP1 and DSP2) control the power flow in the micro-grid by changing the phase shift angles and the duty ratio of the switching devices appropriately.

As can be seen in Fig.1, the EMU includes five computational units. The outputs from voltage and current sensors of the ports are received and recorded in data acquisition and record unit. A communication unit is designed to connect the EMU to the smart-grid control centre through the internet. It receives the required commands for power transfer to/from the grid and metrological data for PV power generation forecasts. A pre-processing unit performs all mathematical calculations and data processing including discretising forecasted energy profiles of the PV and load demand, estimation of the battery SOC and state of hydrogen (SOH). It also performs the MPPT for PV port and the resultant signal is sent to the reference signal generation unit. A fuzzy logic controller (FLC) block defines the appropriate operation mode of the micro-grid according to the long-term energy plans and real-time value of micro-grid parameters. The output from FLC is sent to the mode selection and transition block. Finally, the reference signals for the control loops are generated by the reference signal generation unit according to the selected mode. The real-time data is received with the sampling time of T_n (ranges from milliseconds to seconds) and the long-term predicted data is updated and sampled with the sampling time of T_k (ranges from seconds to minutes). More detail on each computational unit is provided in the next sections.

A. Operation of Pre-processing Unit

As can be seen in Fig.1, the pre-processing unit contains a long-term and a real-time data processor. In this research the PV power generation and load demand profiles are the main uncertain parameters. The PV generation is estimated based on the previously recorded data for the days under the same weather condition. The long-term data pre-processor discretises the predicted profiles of the PV energy and load demand to simplify the analysis of the predicted data and speed up the decision making process. The continuous forecasted profile of the PV power generation ($\tilde{P}_{PV_24h}(t)$) is discretised by using the short-time steps of T_k from

$$\tilde{P}_{PV_24h}(k) = \frac{1}{T_k} \int_{t_0+kT_k}^{t_0+(k+1)T_k} \tilde{P}_{PV_24h}(t) dt \quad (3)$$

where $k \in (0, 1, 2, \dots, \frac{24\text{hours}}{T_k} - 1)$ and $\tilde{P}_{PV_24h}(k)$ is the predicted power generated by PV at the k -th sample and t_0 the prediction starting time. The predicted profile of the load demand, fuel cell and grid energy costs are discretised similarly for 24-hours-ahead.

In this paper, the predicted profile of the load demand is obtained from the average of load demand for the past 30 days with similar conditions using recorded historical data as presented in Fig.8.(a). Comparison of the predicted profile with the actual data shows that the resultant relative

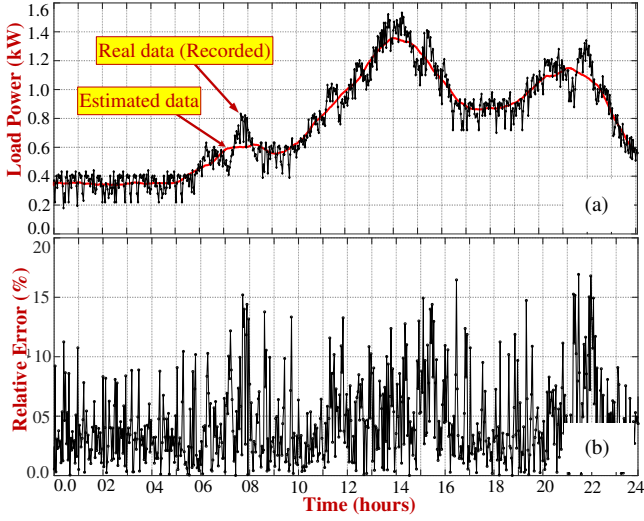


Fig.8.(a) Comparison of measured and estimated load power demand for 24h-ahead, and (b) relative error between measured and estimated values

error for a 24 hours duration time is less than 15 % as can be seen in Fig.8.(b). On the other hand, it is assumed that the energy-cost profile of the main grid is received by the EMU from the regional distribution network control centre and is updated regularly. The fuel cell cost is evaluated by the consumer and is entered into the EMU database when it is required. The fuel cell cost profile should be an almost constant value which is defined according to the fuel cell energy transform efficiency, running cost, and capital cost although it may occasionally need to be updated according to the change in the hydrogen cost. The discretised profiles are further sent to the FLC. The real-time data pre-processor performs the following functions using the real-time value of the micro-grid parameters.

-It estimates the values of SOC and SOH for each sampling time T_n . The battery SOC at n -th sample ($SOC(n)$) is defined from

$$SOC(n) = SOC(n-1) + \frac{T_n}{C_{BT}} [I_{BT}(n) - I_{BT}(n-1)] \quad (4)$$

where C_{BT} is the nominal capacity of the battery bank and $I_{BT}(n)$ the battery current at the n -th sampling time which can be positive during the charge and negative during the discharge process. On the other hand, $SOH(n)$ is estimated by using signals received from the sensors installed in the hydrogen tank.

-It calculates the real-time value of difference between PV power generation ($P_{PV}(n)$) and the load demand ($P_{LD}(n)$) and the difference between real-time values of fuel cell energy cost ($C_{FC}(n)$) and grid energy cost ($C_{GD}(n)$) for short-term fuzzy controller at the n -th sampling time from

$$\begin{aligned} \Delta C(n) &= C_{GD}(n) - C_{FC}(n) \\ \Delta P(n) &= P_{LD}(n) - P_{PV}(n) \end{aligned} \quad (5)$$

-It calculates the real-time value of the PV, battery, load and fuel cell power using voltage and current samples.

-It performs the MPPT process using real-time values of PV voltage based on variable step size incremental conductance (INC) method [42].

IV. STRUCTURE OF FUZZY LOGIC CONTROLLER

As illustrated in Fig.9, the fuzzy logic energy management contains a computational unit, a short-term and

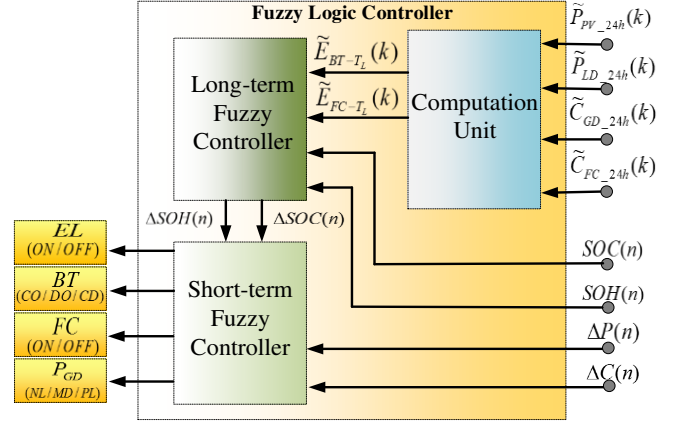


Fig.9. Structure of the proposed fuzzy logic based energy management

a long-term controller. The computational unit calculates the estimated energies that should be supplied or absorbed by the battery (\tilde{E}_{BT-T_L}) and fuel cell (\tilde{E}_{FC-T_L}) during the next moving long-time frame. The estimation is based on the pre-defined long-time energy plans. The resultant values are sent to the long-term fuzzy controller. The long-term fuzzy controller determines the required variation in the available capacity of storage devices (i.e. ΔSOC for battery and ΔSOH for hydrogen tank) to meet the long-term energy plans and send it to the short-term controller. Finally, the short-term fuzzy controller determines the next operation mode of the system based on the required changes in the available capacity of the battery (ΔSOC) and fuel cell (ΔSOH), real-time values of the power difference ($\Delta P(n)$) and energy cost difference ($\Delta C(n)$). The output of the short-term controller is the status of electrolyzer, battery, fuel cell and grid conversion ports. To define the output of the short-term and long-term fuzzy controllers, the max-min product inference and the centre of gravity defuzzification methods are selected [30]. The fuel cell and electrolyzer status is in the form of ON/OFF signal and for the battery is selected as charge only (CO), discharge only (DO) or charge and discharge (CD). In the case of energy transfer to/from the grid, a variable quantity in the range of negative large (NL), medium (MD) and positive large (PL) is selected.

The output signals from the fuzzy controller are sent to the mode selection and transition unit to extract the appropriate operation mode. More detail on each unit of the FLC block is provided in the following sections.

A. Operation of Computational Unit

This section provides the details of the computational unit. As can be seen in Fig.8, the computational unit estimates the values of energies that need to be supplied or absorbed by battery, $\tilde{E}_{BT-T_L}(k)$ and supplied by fuel cell, $\tilde{E}_{FC-T_L}(k)$ during the prediction moving time-frame T_L . The length of the moving time-frame T_L , ranges from tens of minutes to a few hours. The estimated values are updated at the beginning of each time-step T_k by moving the time-frame T_L one time-step ahead (considering that $T_L = mT_k$). The estimation is performed for each sampling time T_k according to the long-term energy plan rules. In this paper, the long-term energy plan rules can be briefly listed as:

- In all operation modes, the PV is given priority as the source of energy for supplying the load, and the surplus

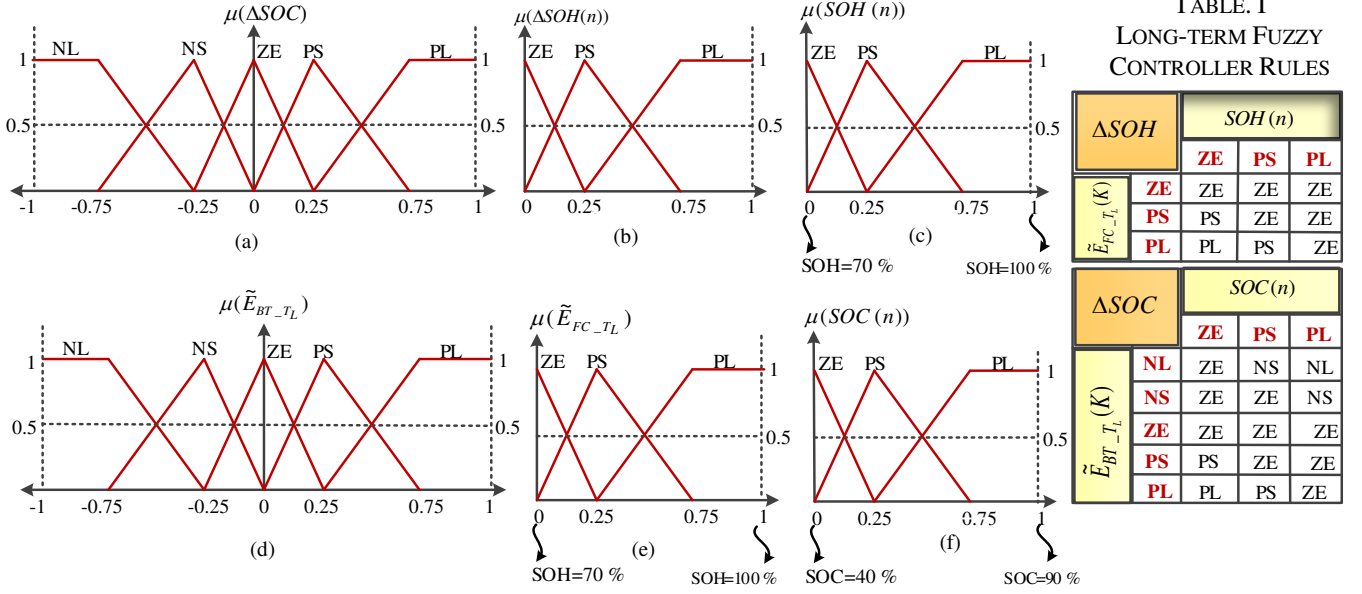


Fig.10. The membership function of the long-term fuzzy controller, (a) $\Delta SOC(n)$ (b) $\Delta SOH(n)$ (c) $SOH(n)$ (d) \tilde{E}_{BT-T_L} (e) \tilde{E}_{FC-T_L} and (f) $SOH(n)$

energy is preferred to be used to charge the battery (if required). The second option is the main grid which requires the acknowledgment of request by the regional distribution network control centre. The last option is supplying shiftable loads, water heating systems, and dump loads.

- When the predicted PV power generation is less than the predicted load demand, the difference can be covered by the battery, fuel cell, and/or grid depending on the amount of required power taking into account the energy cost and availability and the maximum power of each energy source. According to the proposed management technique, the small values of the difference between the PV generation and load demand should be covered by the battery and/or grid depending on the availability and cost of energy. If the difference is more than the battery capacity and less than the fuel cell, it should be covered by the grid and/or fuel cell depending on their energy cost. The SOC and SOH levels and their limitations should be taken into account for each sampling time.

- The battery capacity can be managed according to the SOC level as

$$\begin{cases} \text{Bus stabilization only} & 0.9 < SOC < 1 \\ \text{Storage and bus stabilization} & 0.4 < SOC < 0.9 \\ \text{Off-grid operation} & 0.1 < SOC < 0.4 \end{cases} \quad (6)$$

Finally, the estimated energy that should be exchanged with the battery ($\tilde{E}_{BT-T_L}(k)$) or supplied by the fuel cell ($\tilde{E}_{FC-T_L}(k)$) during the moving time-frame T_L can be estimated by

$$\tilde{E}_{BT-T_L}(k) = \sum_k^{k+m} T_k \tilde{P}_{BT-T_k}(k) \quad (7)$$

$$\tilde{E}_{FC-T_L}(k) = \sum_k^{k+m} T_k \tilde{P}_{FC-T_k}(k) \quad (8)$$

The resultant values of $\tilde{E}_{BT-T_L}(k)$ and $\tilde{E}_{FC-T_L}(k)$ are used as the input variables to the long-term fuzzy controller.

B. Design of the Long-term Fuzzy Controller

The long-term fuzzy controller defines the desired variation in the SOC and SOH levels (presented as ΔSOC , ΔSOH respectively) to meet the long-term energy plans by using estimated values of energies that should be supplied or absorbed by battery and fuel cell (\tilde{E}_{BT-T_L} and \tilde{E}_{FC-T_L}) and

the real-time value of SOC and SOH ($SOC(n), SOH(n)$) (referring to Fig.9). Table.I, illustrates the linguistic rules of the long-term fuzzy controller for determining ΔSOC and ΔSOH . Fig.10 shows the membership functions of the input and output variables of the long-term fuzzy controller. As illustrated in the figure, the linguistic variables of the membership functions are abbreviated as negative large (NL), negative small (NS), zero (ZE), positive small (PS), and positive large (PL). All membership functions are normalized according to the maximum and minimum values of their variable. As an example, when \tilde{E}_{BT-T_L} is high and

positive (PL), this means that high amounts of energy should be supplied by the battery during the next long time-frame to meet the long-term energy plan. In this case, if the real-time value of SOC is high (PL) so there is no need for change in the SOC and therefore, ΔSOC should be equal to zero (ZE). On the other hand, when \tilde{E}_{BT-T_L} is (PL) but the current value of SOC is low (ZE) then there is need to increase the SOC level during the next operation mode to meet the desired level (subject to complying with the other conditions). Therefore, ΔSOC should be positive and high (PL). This will increase the stored energy in the battery for the next hours to supply the load or transfer energy to the grid. Other fuzzy control rules are following the same principles.

C. Design of the Short-term Fuzzy Controller

The short-term fuzzy controller, which is the main decision maker of the EMU operates based on the real-time information of the system including the difference between PV power generation and load demand, $\Delta P(n)$, the

TABLE. II
FUZZY RULES OF SHORT-TERM CONTROLLED

INPUT VARIABLES								OUTPUT VARIABLE							
$\Delta P(n)$	$\Delta C(n)$	$\Delta SOC(n)$	$\Delta SOH(n)$	BT	FC	EL	$P_{GD}(n+1)$	$\Delta P(n)$	$\Delta C(n)$	$\Delta SOC(n)$	$\Delta SOH(n)$	BT	FC	EL	$P_{GD}(n+1)$
PL	PL	PL	PL	CD	OFF	OFF	NL	ZE	ZE	ZE	PS	CD	OFF	OFF	MD
PL	PL	PL	PS	CD	ON	OFF	MD	ZE	ZE	NL	PL	CD	OFF	OFF	MD
PL	PL	ZE	PL	CD	OFF	OFF	NL	ZE	ZE	NL	PS	CD	OFF	OFF	MD
PL	PL	ZE	PS	CD	ON	OFF	MD	ZE	NL	PL	PL	CO	OFF	ON	NL
PL	PL	NL	PL	DO	OFF	OFF	MD	ZE	NL	PL	PS	CO	OFF	OFF	NL
PL	PL	NL	PS	DO	ON	OFF	MD	ZE	NL	ZE	PL	CD	OFF	ON	NL
PL	ZE	PL	PL	CO	OFF	OFF	NL	ZE	NL	ZE	PS	CD	OFF	OFF	MD
PL	ZE	PL	PS	CO	ON	OFF	NL	ZE	NL	NL	PL	CD	OFF	ON	NL
PL	ZE	ZE	PL	DO	OFF	OFF	MD	ZE	NL	NL	PS	CO	OFF	OFF	MD
PL	ZE	ZE	PS	DO	ON	OFF	MD	NL	PL	PL	PL	CO	ON	OFF	MD
PL	ZE	NL	PL	DO	OFF	OFF	NL	NL	PL	PL	PS	CO	ON	OFF	PL
PL	ZE	NL	PS	DO	ON	OFF	MD	NL	PL	ZE	PL	CD	OFF	ON	MD
PL	NL	PL	PL	CO	OFF	ON	NL	NL	PL	ZE	PS	CO	ON	OFF	PL
PL	NL	PL	PS	CO	OFF	OFF	NL	NL	PL	NL	PL	DO	OFF	ON	PL
PL	NL	ZE	PL	CD	OFF	ON	NL	NL	PL	NL	PS	DO	ON	OFF	PL
PL	NL	ZE	PS	CD	OFF	OFF	NL	NL	ZE	PL	PL	CO	OFF	OFF	MD
PL	NL	NL	PL	DO	OFF	ON	NL	NL	ZE	ZE	PL	CD	OFF	ON	MD
PL	NL	NL	PS	DO	OFF	OFF	NL	NL	ZE	ZE	PS	CD	OFF	OFF	PL
ZE	PL	PL	PL	CD	OFF	OFF	MD	NL	ZE	NL	PL	CO	OFF	ON	MD
ZE	PL	PL	PS	CO	ON	OFF	MD	NL	ZE	NL	PS	CO	OFF	ON	MD
ZE	PL	ZE	PL	CD	OFF	OFF	MD	NL	ZE	NL	PS	DO	OFF	OFF	PL
ZE	PL	ZE	PS	DO	ON	OFF	MD	NL	NL	PL	PL	CO	OFF	ON	MD
ZE	PL	NL	PL	DO	OFF	OFF	PL	NL	NL	PL	PS	CO	OFF	OFF	MD
ZE	PL	NL	PS	DO	ON	OFF	PL	NL	NL	ZE	PL	CD	OFF	ON	MD
ZE	ZE	PL	PL	CD	OFF	OFF	MD	NL	NL	ZE	PS	CO	OFF	OFF	PL
ZE	ZE	PL	PS	CO	ON	OFF	MD	NL	NL	NL	PL	DO	OFF	ON	MD
ZE	ZE	ZE	PL	CD	OFF	OFF	MD	NL	NL	NL	PS	CO	OFF	OFF	PL

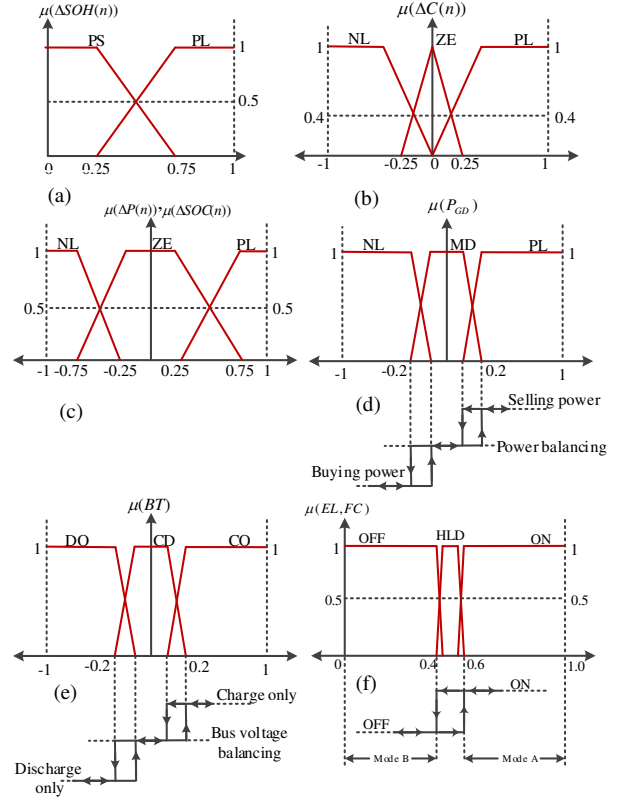


Fig.11. Membership function of short-term fuzzy controller (a) $\Delta SOH(n)$ (b) $\Delta C(n)$ (c) $\Delta P(n), \Delta SOC(n)$ (d) $\mu(P_{GD})$ (e) $\mu(BT)$ and (f) $\mu(EL, FC)$

difference between the cost of grid and fuel cell energies $\Delta C(n)$, and required variations in the SOC and SOH levels ($\Delta SOC(n)$ and $\Delta SOH(n)$). The input variable $\Delta SOC(n)$ is the important factor to define the battery status, $\Delta SOH(n)$ to define the status of the electrolyzer, $\Delta C(n)$ to make a decision between grid and fuel cell due to their energy cost and $\Delta P(n)$ to define the amount of the energy difference and the source that can supply or absorb it. The operation status of the battery, fuel cell and electrolyzer and the amount of power that should be sent to, or received from the main grid are sufficiently defined by using the real-time value of the above parameters. The resultant outputs are sent to the mode selection and transition unit and further used to select the operation mode of the system.

The short-term fuzzy controller rules are defined according to the energy management scenarios and control objectives and in this paper, are almost the same as those are defined in computation unit. The main difference is that they are based on real-time data which are updated for each sampling time n . In brief, the electrolyzer is activated during the low-cost grid energy periods. The battery can be charged by the fuel cell, PV or grid depending on the availability and energy cost and is discharged under light load when its energy is cheaper than the main grid. It also is activated at peak demand hours to supply the load or transfer power to the grid. In this paper, the sampling time of the short-term fuzzy controller (T_n) is 100 ms. Therefore, the operation mode of the micro-grid is updated with the frequency of 10 Hz. In the case of any change in the operation mode, it is applied to the device level controllers, otherwise, the system remains in the current operation mode. The short-term fuzzy control rules are illustrated in Table.II and the membership functions are presented in Fig.11.

The input membership functions are designed and normalized almost similar to the long-term controller and are classified in the range of NL, NS, ZE, PS, and PL. In the case of output variables, the status of the fuel cell and electrolyser can be either ON or OFF and the function HOLD is used as a hysteresis function to reduce the mode fluctuations in the boundary conditions. The battery status can be charge only (CO), discharge only (DO) and charge and discharge (CD) or standby mode where the battery is used to stabilize the dc bus voltage in transients and compensate for the low dynamic response of the fuel cell. The output power membership function defines the amount and the direction of power transfer to/from the main grid. The membership functions are positive large (PL) for selling power to the grid, Negative large (NL) for buying power from the grid and medium (MD) for flexible power transfer to/from the main grid. Similarly, a hysteresis function is also considered between the different statuses of output membership functions. The added hysteresis zones are mainly effective in the system level control and selection of the operation modes. They are applied to the output membership functions to avoid undesirable oscillations in the status of the micro-grid elements and consequently the system operating modes. Therefore, the variation in the output variable of the short-term fuzzy controller at the boundary of two adjacent statuses should exceed a threshold level (determined by hysteresis band) to result in a change in the micro-grid operation mode. The proposed hysteresis functions cannot make any instability in the closed loop control of the converters as operation mode status is updated every 100 ms ($f=10$ Hz) which is much more than the device level controller's dynamic response.

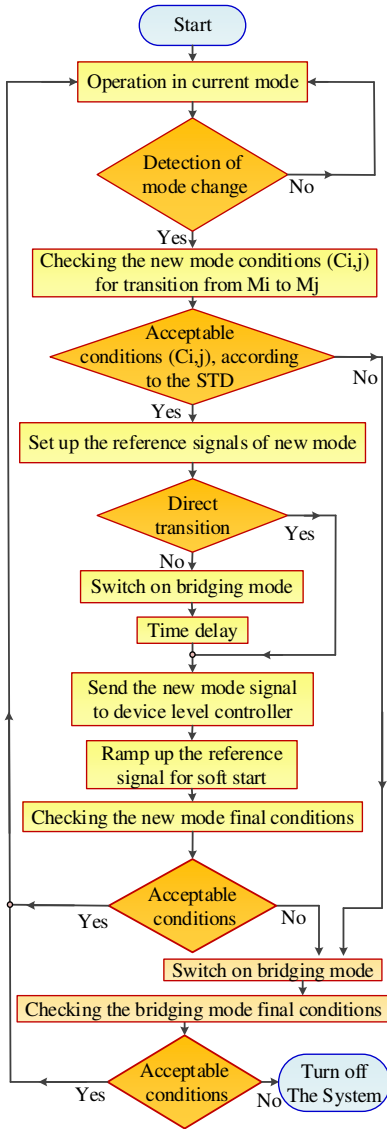


Fig.14. Flowchart of mode transition unit (MTU) operation

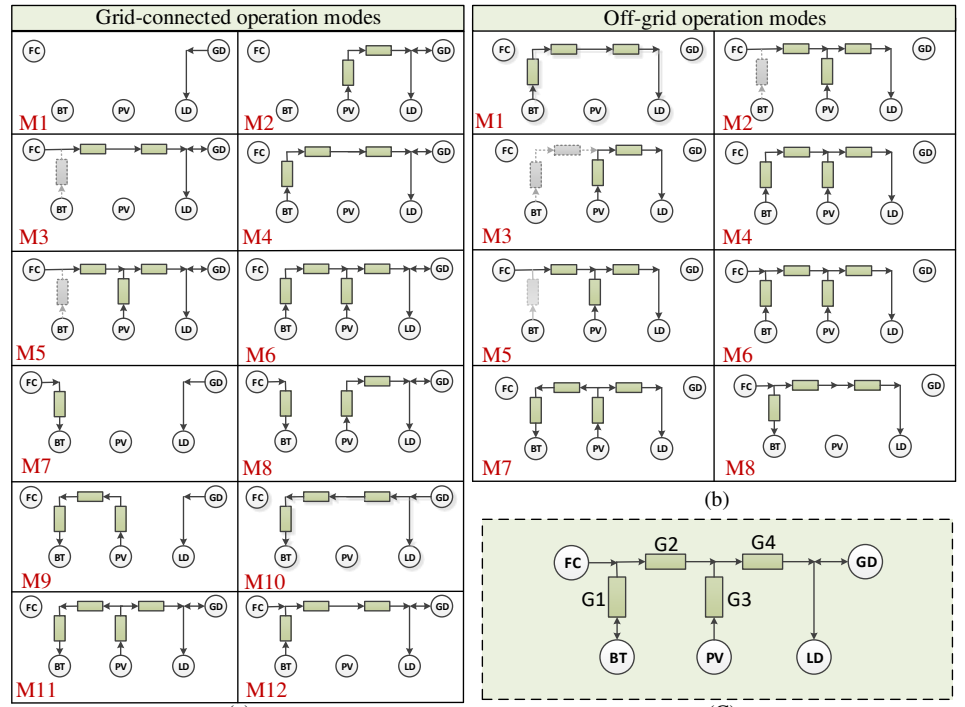


Fig. 12. Operation modes of the proposed micro-grid, (a) grid-connected, (b) off-grid modes, and (c) basic power flow model

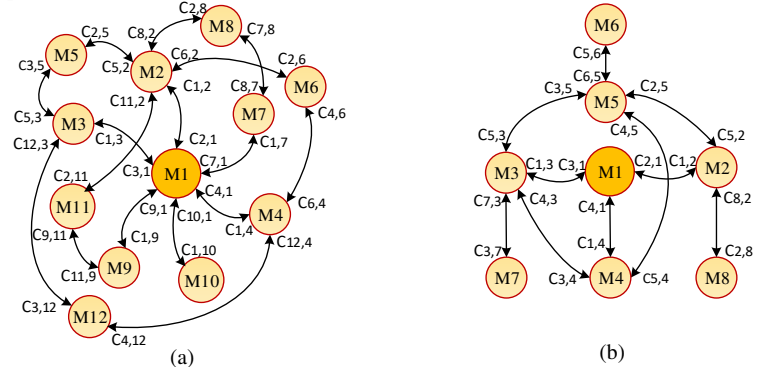


Fig. 13. State transition diagram of mode transition unit in (a) grid connected and, (b) islanded operation modes

V. MODE SELECTION AND TRANSITION UNIT

Mode transition is a common problem in micro-grids with ac or dc electrical bus and generates undesirable instabilities in voltage and frequency [51]. The problem is much less in the case of using the magnetic bus if an appropriate mode transition strategy is designed due to the large number of operation modes. In this paper, a mode selection and transition unit (MSTU) is designed to control and smooth the mode transition process. The transition path between different operation modes depends on the several factors such as current and destination operation modes and the systems conditions. In the case that direct transition is not possible, a bridging mode is required for the smooth transition. On the other hand, some conditions such as maximum charging and discharging power of the battery and fuel cell should be taken into account. The system operation modes are different for the grid-connected and islanded conditions. As presented in Fig.12 (a) and (b), the proposed micro-grid is able to operate in 12 grid-connected and 8 islanded modes. The operation modes are presented based on the basic topology illustrated in Fig.12. (c), where G_1 - G_4 represent the gain of conversion blocks. The mode

M1 is selected as the basic mode in grid-connected condition as the load is always connected to the grid and therefore, it is common between all grid-connected operation modes. The battery link is presented in gray colour in the standby condition. In the mode M2, the PV and grid are supplying the load and this happens when the load demand is more than the PV generation. The operation of other modes can be readily defined using the arrows that represent the power flow direction. In the case of islanded operation condition, the battery is the only source that is always connected to the load or is in the standby mode. Therefore, M1 is selected as the basic mode and is used as the bridging mode during the mode transition. The MSTU operates according to a state transition diagram (STD) which defines the appropriate transition paths between the operation modes and the required actions and conditions. Fig.13 shows the STD for both grid-connected and islanded operation conditions. The mode transition conditions which allow passage from mode M_i to M_j are presented as $C_{i,j}$ in the STD and contain the required test parameters for mode transition. The test parameters are mainly those already used in the real-time fuzzy controller for decision making. They are used to determine the availability and status of energy in

supplying source, energy demand in absorbing elements and available capacity in storage devices in the destination mode elements. The most commonly used parameters are the real-time value of voltage and current of the destination mode elements, SOC and SOH. Details of the test parameters for each individual transition path are not presented due to their similarity and the large number of transition paths (totally 50 grid-connected and off-grid paths). Fig.14 illustrates the flowchart of mode transition process. As can be seen, the mode transition process starts with mode-change detection from output variables of the FLC. The conditions of the new mode such as output voltage and energy capacity of sources in the new mode are checked and in the case of acceptable conditions, the mode transition process starts. The process starts with setting up the reference signals of the control loops in the device level controller according to the new mode requirements. The system may need to be switched on a bridging mode before moving to the new operation mode. A time delay is applied to stabilize the bridging mode conditions. The new mode command is sent to the device level controller to start sending the PWM signals to the switching devices of the new active ports. It should be noticed that the duty ratio is minimized due to the soft start operation and the reference signals of the control loops being small. To activate the new ports, the reference signals ramp up to the nominal value and then the conditions of the new mode are checked. In the case of acceptable conditions, the mode transition process is ended by moving to the normal operating conditions. In the case of any unexpected condition, the system switches on the bridging mode and remains in this mode as long as bridging-mode conditions are satisfactory otherwise the system is turned off.

VI. VALIDITY TEST OF THE ENERGY MANAGEMENT UNIT

A prototype of the proposed micro-grid is designed and implemented as presented in Fig.15 (a) and (b). Two DSP controllers (C2000/TMS320F28335) are used as device level controller. The system level control (energy management and operation mode control) is performed by a PC using MATLAB graphical user interface (GUI). It also performs the system monitoring and data record during the energy management process. Two sensor and protection boards are designed to receive the signals of the converter ports through Hall effect voltage (LV 25-P) and current (LTSR25-NP) sensors. The MPPT reference signal generated by EMU is sent to the DSP1 to control the duty ratio of the switching devices at the PV port and is updated every 10 ms ($f=100$ Hz). The single-phase inverter is implemented using H bridge units made by SEMIKRON (SK30GH123) with isolated drivers (SKHI20opA). The H-bridge units of the TAB converter are designed using IGBT switches (IRG7PH42) and integrated driver circuit (VLA567-01R) and optoisolators (6N136). Both DSPs are connected to the signal conditioning and level shifters on the control and interface board and further to the EMU.

The operation of MSTU in direct and indirect mode transitions is presented in Fig.16. In the direct mode transition from M5 to M3, presented in Fig.16 (a), when the PV power is approached to zero, the fuel cell undertakes to supply the difference, and the battery operates as compensator. In the indirect mode transition from M2 to M3, presented in Fig.16 (b), the mode M1 is used as

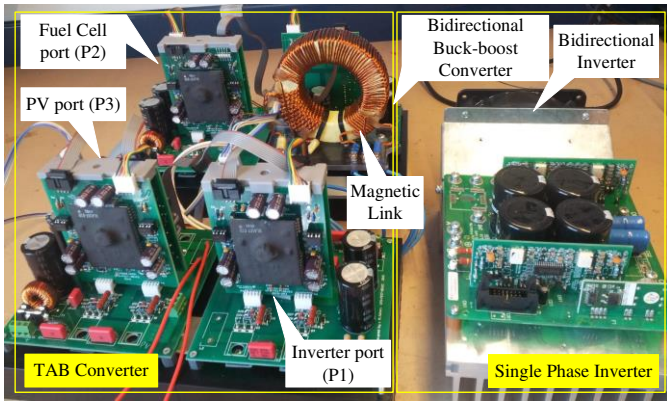
bridging mode to leave enough time for fuel cell start-up. The fuel cell emulator parameters are selected according to the available commercial model [52]. Fig.17 shows the experimentally measured waveforms of voltages and currents generated by the H-bridge units of the TAB converter applied to the magnetic link for two cases of duty cycle and phase shift angles, ($D=0.6$, $\varphi_{21}=\pi/5$, $\varphi_{31}=\pi/3$, and $D=0.8$, $\varphi_{21}=\pi/3$, $\varphi_{31}=\pi/5$). Fig.18 presents the waveforms of the inverter output voltage and current. As can be seen, the inverter current follows the grid voltage with unity power factor and the resultant THD when the output power equals 1.7 kW, is about 3.27 % and frequency deviation less than 0.5 %. This is in the acceptable range according to the Australian (AS/NZS4777) and international (IEEE 1547 and IEC 61727) standards for grid-connected renewable energy systems [43], [44].

To study the energy management process, the residential load is implemented by parallel connection of two groups of variable and constant loads as presented in Fig.15 (b). The constant loads are used to model permanent residential loads such as refrigerator, lighting and the variable section is used to model the random and short duration loads. The experimental test for each scenario is carried out for a time duration of 2 hours to model a 24 hours residential load which starts at 12 AM. Therefore every 2 minutes in the 24-hour time period is modelled by a 10 seconds time step in the actual test. According to this, 720 samples with time duration of 10 seconds are used to record the parameters of the proposed micro-grid ($T_L=40$ min, $T_k=10$ s and $T_n=100$ ms). The experimental test is carried out for the proposed micro-grid and the objective of the proposed energy management scenario is minimizing the purchasing power from the grid at peak hours and sending energy to the grid during the peak hours when the grid energy cost is high. The experimental test was performed for three different scenarios.

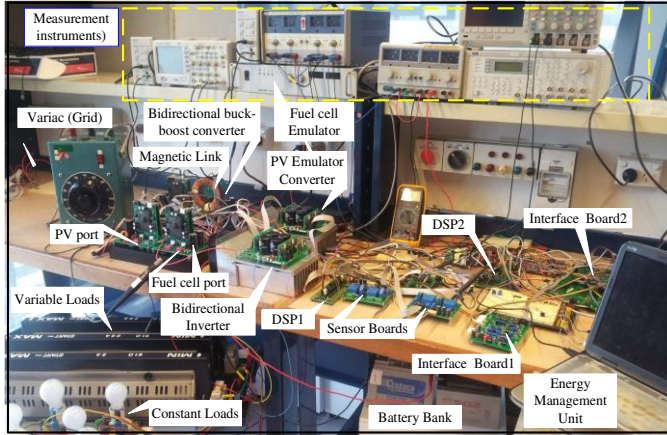
The PV output power profile in the first scenario is changed according to a normal sunny day condition. The system is assumed to be in the grid-connected mode with flexible power flow to/from the grid. In the second scenario, the PV power profile is changed to model the cloudy condition with variable irradiation level. In the third case, the proposed micro-grid operates in off-grid conditions with the fuel cell, PV and battery as input sources. Following sections provide more details on the operation of EMU for the proposed energy management scenarios.

A. Energy Management in Grid-connected Condition

The power profiles of the PV generation, load demand, energy cost profiles of the fuel cell, battery and grid, and the estimated values of SOC and SOH for 24-hours duration are presented in Fig.19.(a). The difference between PV generation and load demand, grid power, fuel cell power and the battery power profiles for the same duration time are presented in Fig.19.(b). As can be seen in the energy cost profiles, the cost of fuel cell and battery energies follow a constant value during the day while the cost of grid energy is variable with the time. The maximum power of the battery during charge is limited to 250 W and discharge to 300 W and the fuel cell maximum power in the grid-connected mode is limited to 350 W and in off-grid to 450 W. The operation modes of the proposed micro-grid for the

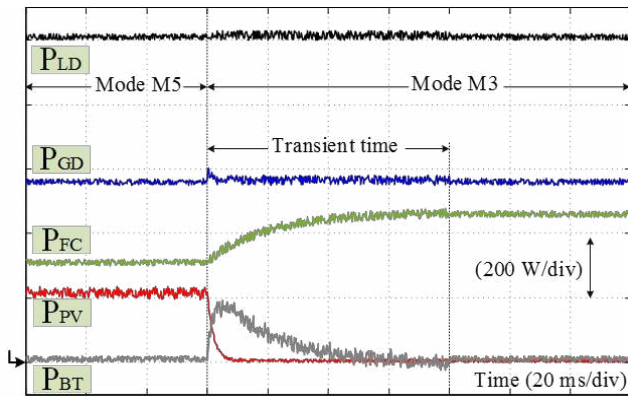


(a)

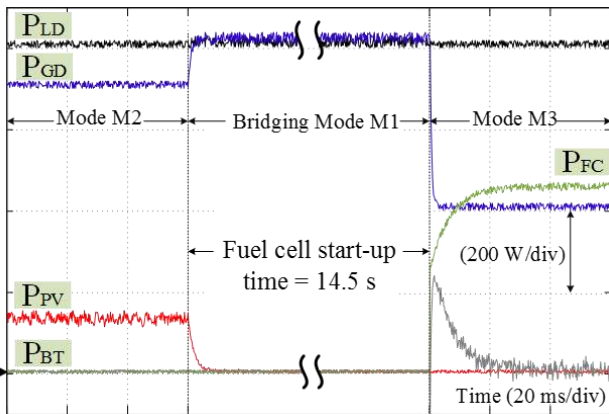


(b)

Fig.15. Experimental set of proposed micro-grid (a)-multi-port converter and single phase bi-directional inverter and (b)-proposed micro-grid under the test

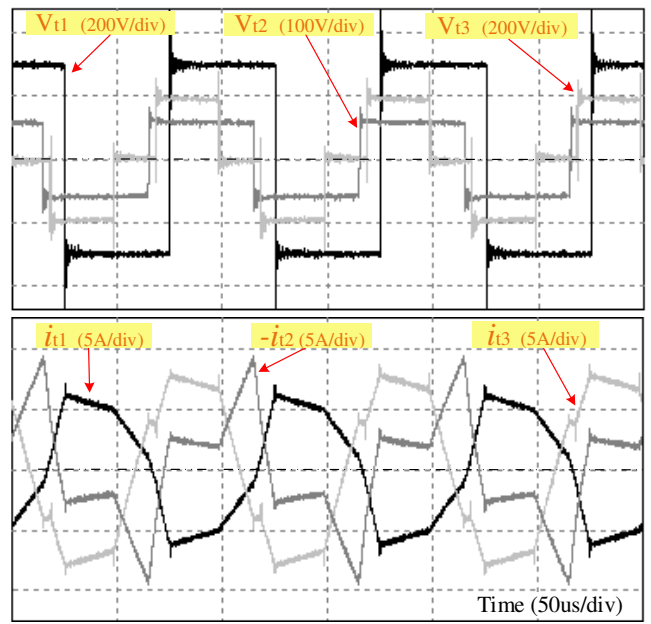


(a)

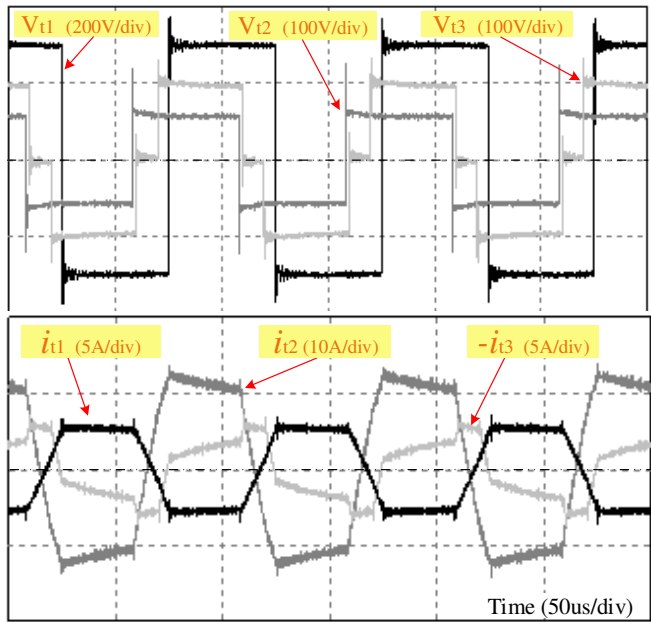


(b)

Fig.16. Operation of MSTU for two cases (a)-direct node transition from M5 to M3, and (b) indirect mode transition from M2 to M3 and using M1 as bridging mode



(a)



(b)

Fig.17. The TAB converter voltage and current waveforms for two cases (a), $D=0.6$, $\phi_{21}=\pi/5$, $\phi_{31}=\pi/3$, and (b), $D=0.8$, $\phi_{21}=\pi/3$, $\phi_{31}=\pi/5$.

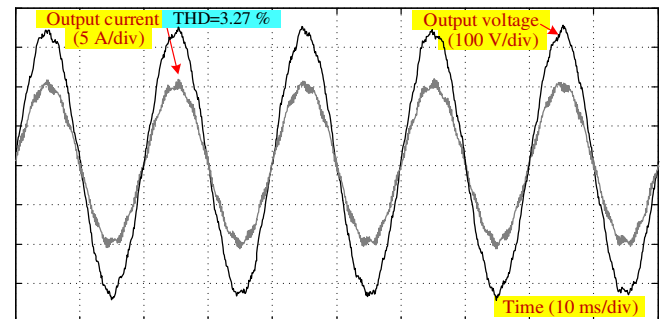


Fig.18. Experimental waveforms of inverter voltage and current

24-hours' time duration of the experimental test are presented at the bottom of the figure.

As can be seen in the figure, for the first time interval starting from t_1 to t_2 there is no power generated by PV and due to the small amount of load demand, it can be supplied by either battery or grid. As the cost of the battery energy is

less than the grid for the proposed time interval, it is selected to supply the load and operation mode of the system selected as mode 4 (M4). At $t=t_2$ the cost of grid energy is reduced to less than the battery which means that using the grid is more beneficial compared to the battery and the operation mode is changed to M1. It should be noted that the battery still has enough capacity to supply the load demand if it is required (referring to the SOC level variation graph). When the PV panel starts to generate power at $t=t_3$, the PV port needs to be activated and the operation mode changes to M2. This operation mode continues as long as the PV power is less than load demand.

At $t=t_4$ where PV generation is more than load demand, the surplus energy can be transferred to one of the controllable loads, grid or battery. According to the long-term energy plan, the battery needs to be charged for the next long-time interval and the actual level of SOC is less than the desired value. Therefore, the battery is selected to be charged and the operation mode is changed to M11. Due to the limit in the battery charging power, the additional energy is sent to the main grid. At $t=t_5$, the battery is charged to the full capacity and SOC reaches the maximum level of allocated capacity of the battery for operation as storage (SOC=90%). The surplus energy should be supplied to the grid although, in the case of PV generation less than load demand, the battery is preferred to supply the load due to its lower energy cost compared with the grid. Therefore, the system operation mode is changed to M6 where both battery and PV can supply the load and additional energy is transferred to the grid. At $t=t_6$, the load demand is more than the PV and battery powers and it is required for either the fuel cell or grid to supply the difference. Considering the energy cost of the fuel cell and grid at this time, the fuel cell is selected as the preferred source. In this case fuel cell operates with a constant output power and the difference between load demand and fuel cell power is compensated by the battery. As fuel cell and battery are connected directly to the same dc bus, it is easy for the battery to be charged or discharged into the dc bus to compensate for the load demand variations. Therefore, during t_6 to t_7 , the system operation mode changes to M5 where the fuel cell power is more than the load demand and the surplus energy of fuel cell charges the battery. At $t=t_7$, the load demand changes to more than fuel cell power which requires the battery to supply the difference and the operation mode is changed to M12. At $t=t_8$, the cost of grid energy decreases to less than the battery and fuel cell. Therefore, the operation of the fuel cell and the battery is not economic and the load should be supplied by the grid. The system operation mode changes to the basic mode M1 where grid is the only energy source of the micro-grid system.

The total energy supplied or received by each element can be calculated by using its daily power profile. As an example, energy supplied by PV can be determined by

$$E_{PV_24h} = \sum_{k=1}^{720} P_{PV}(k)T_k = T_k \sum_{k=1}^{720} P_{PV}(k) \quad (9)$$

The fuel cell energy (E_{FC_24h}) and the load energy (E_{LD_24h}) are defined similarly. On the other hand, the energy received by battery in charging mode ($E_{BT_24h}^{CHD}$), or supplied by the battery in discharging mode ($E_{BT_24h}^{DCH}$) can be determined by

$$\begin{cases} E_{BT_24h}^{CHD} = \sum_{k=1}^{720} P_{BT_24h}(k)T_k & \text{where } P_{BT_24h}(k) < 0 \\ E_{BT_24h}^{DCH} = \sum_{k=1}^{720} P_{BT_24h}(k)T_k & \text{where } P_{BT_24h}(k) \geq 0 \end{cases} \quad (10)$$

The energy sold to the grid ($E_{BT_24h}^{SEL}$) and the energy supplied by the grid ($E_{BT_24h}^{BUY}$) can be defined similarly to the battery. The energy loss in the system is determined from

$$E_{LS_24h} = E_{PV_24h} + E_{FC_24h} + E_{GD_24h}^{BUY} - E_{GD_24h}^{SEL} + \Delta E_{BT_24h} \quad (11)$$

where the variation in the battery energy ΔE_{BT_24h} during the 24h time duration can be found by

$$\Delta E_{BT_24h} = E_{BT_24h}^{DCH} - E_{BT_24h}^{CHD} + E_{BT_0h} - E_{BT_24h} \quad (12)$$

where E_{BT_0h} and E_{BT_24h} are the stored energy in the battery at the beginning and at the end of the 24h time interval, respectively, and can be determined from the estimated values of SOC at the beginning and end of the time interval. The energy loss in the system is mainly related to the switching and conduction losses in the dc-dc converters and inverter. Fig.20 (a), illustrates the energy analysis of the micro-grid for the first energy management scenario during the 24-hour time-duration. It can be seen that almost 60% of the load energy is provided by PV while fuel cell, battery and grid-supplied almost 15% of the total load demand. It can be seen that the energy received from the grid is 1 kWh on average which is much less than actual load consumption (8.6 kWh). To analyse the operation of micro-grid from the economic point of view, the total cost of the energy supplied, stored or consumed by each element is calculated as presented in Fig.20 (b). To calculate the total cost of energy for 24 hours duration, the amount of power and the real-time value of energy are taken into account. For example, the PV energy cost for the 24 hour time period can be calculated from

$$C_{PV_24h} = \sum_{n=1}^{720} P_{PV_24h}(k)C_{PV}(k)T_k \quad (13)$$

In this paper, the PV energy cost is assumed to be 0.02 \$/kWh, the fuel cell energy cost is 0.3 \$/kWh, the battery cost is 0.10 \$/kWh and the grid cost is varying from 0.05 to 0.50 \$/kWh. The energy cost analysis can be used to compare the customer benefits from the renewable energy system for a particular time duration such as a day, week, month, or a year. Looking at the energy cost graph shows that the customer benefits from supplying energy to the grid at peak demand hours when the grid energy cost is high is 0.925 \$/day. This can compensate for the energy cost resulting from other sources. About 60% of the total energy cost of the load belongs to the fuel cell compared to the other sources (0.45 \$/day).

In the second energy management scenario, the operation of the proposed energy management system is studied under the cloudy weather condition where the PV output power is changed abruptly. Fig.21 (a) illustrates the PV output power profile for the second scenario. As can be seen, the PV output is dropped due to the shading effects and consequently, different operation modes are required compared to the previous case. The load demand and energy

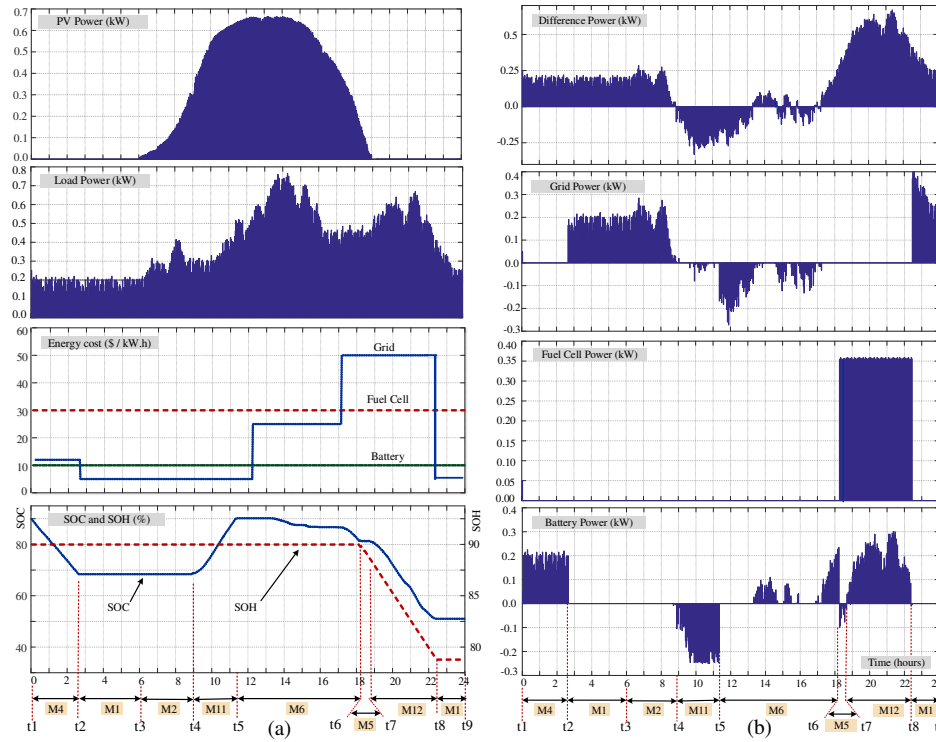


Fig.19. Profiles of the PV power generation, load power demand, energy cost and SOC/SOH levels, difference between PV power generation and load power demand, grid power, fuel cell power and the battery power for a sunny day profile and grid-connected condition.

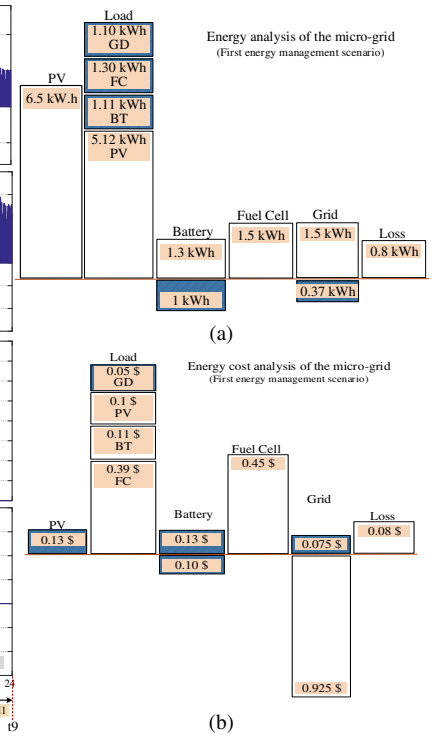


Fig.20. (a) Energy distribution and (b) energy cost analysis of the proposed micro-grid for a sunny day profile and grid connected mode

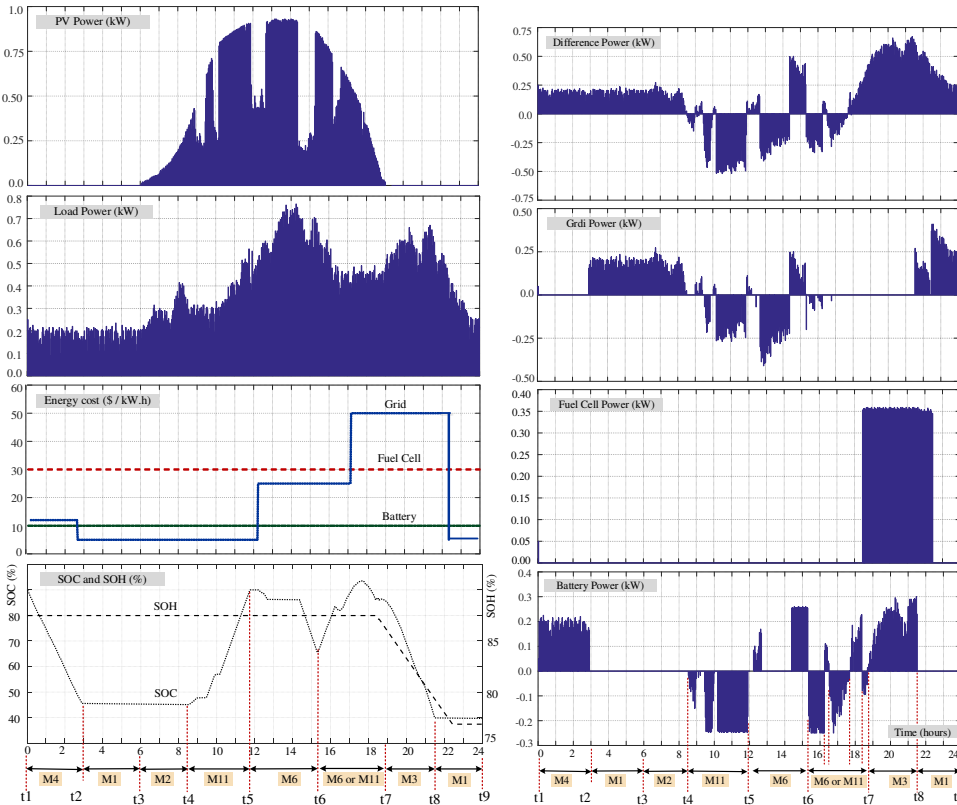


Fig.21. Profiles of the PV power generation, load power demand, energy cost and SOC/SOH levels, difference between PV power generation and load power demand, grid power, fuel cell power and the battery power for the cloudy day profile and grid connected mode

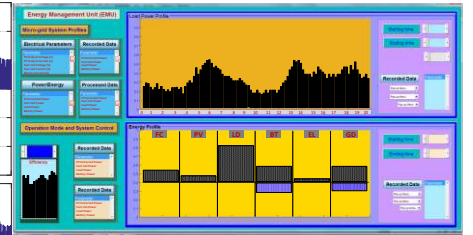


Fig.22. The designed graphical user interface (GUI) using MATLAB for energy management and data monitoring of the proposed micro-grid (including the micro-grid system recorded data of electrical parameters, power and energy profiles and processed data) and operation mode and system control menu (including history of operation modes, system faults and input data setting).

cost profiles are changed with an almost similar pattern to the first scenario while the resulting variations in the battery SOC and SOH levels are different due to the new operation modes. The difference between PV and load power, battery, fuel cell and load power profiles are presented in Fig.21 (b) and discussion on the different operation modes can be carried out similar to the previous scenario. The presented

data is obtained from the recorded data in the EMU using graphical user interface (MATLAB/GUI) as presented in Fig.22.

B. Energy Management in Off-grid Condition

In the third energy management scenario, the operation of the proposed EMU in off-grid conditions is studied. In this

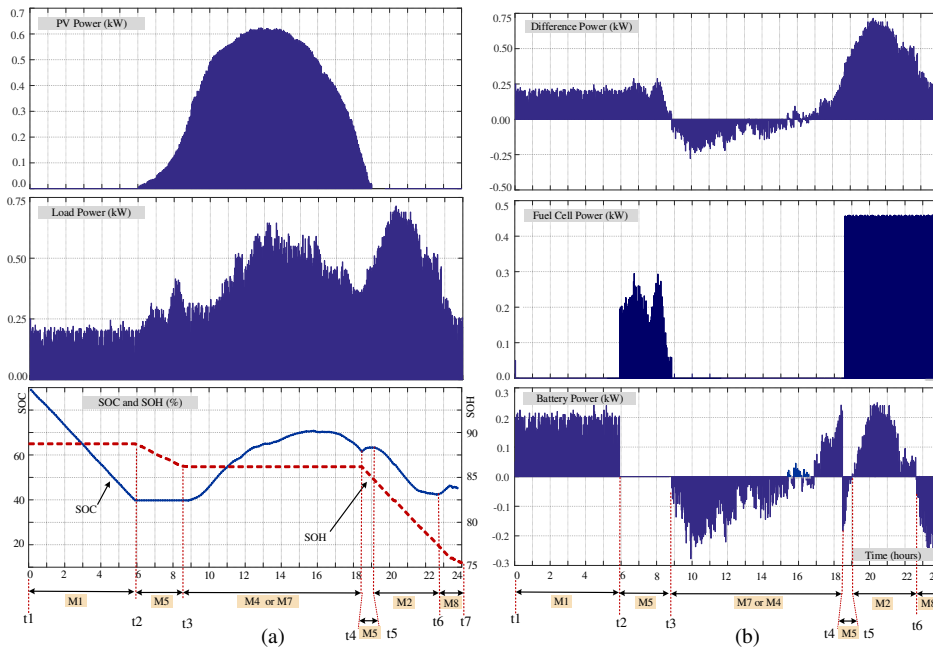


Fig. 23. Profiles of the PV power generation, load power demand, energy cost and SOC/SOH levels, difference between PV power generation and load power demand, grid power, fuel cell power and the battery power for a sunny day profile and off-grid condition.

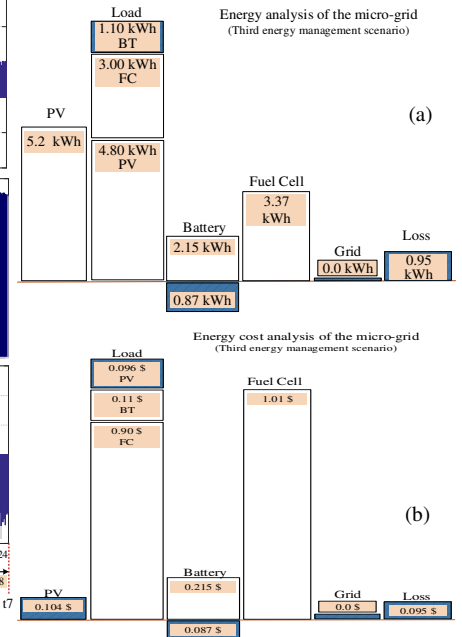


Fig. 24. (a) Energy distribution and (b) energy cost analysis of the proposed micro-grid for a sunny day profile and off-grid condition.

Grid-connected mode		Islanded mode	
Without Renewable	With Renewable	Without Renewable	With Renewable
0.4 kW.h 0.12 \$/kW.h	1.1 kW.h GD: 0.05 \$/kW.h	0.5 kW.h 0.12 \$/kW.h	1.10 kW.h BT: 0.10 \$/kW.h
2.6 kW.h 0.25 \$/kW.h	5.12 kW/h PV: 0.02 \$/kW.h	2.5 kW.h 0.25 \$/kW.h	3.00 kW.h FC: 0.30 \$/kW.h
2.63 kW.h 0.5 \$/kW.h	1.11 kW.h BT: 0.10 \$/kW.h	2.68 kW.h 0.5 \$/kW.h	4.8 kW.h PV: 0.02 \$/kW.h
3 kW.h 0.05 \$/kW.h	1.30 kW.h FC: 0.30 \$/kW.h	3.16 kW.h 0.05 \$/kW.h	
Total cost: 2.163 \$/day	Total cost: 0.66 \$/day	Total cost: 2.18 \$/day	Total cost: 1.10 \$/day

Fig. 25 Comparison of energy costs of proposed residential load for three cases, grid-supplied only, grid-connected with renewable sources and off-grid with renewable sources

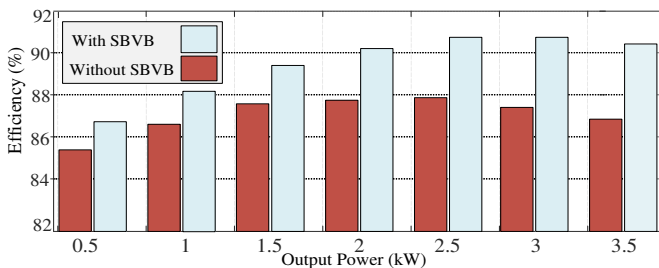


Fig. 26 The total efficiency of the system with and without using SBVB technique

case, the proposed micro-grid is disconnected from the main grid and is supplied only by the PV, fuel cell and battery. The PV power profile is changed according to a sunny day pattern and the load demand profile is slightly different from that of grid-connected mode. It is assumed that the energy cost of the battery is constant and less than fuel cell for entire test duration and PV is the cheapest as the preferred

source. Therefore, it is not necessary to present the energy cost profile.

The operation modes and power profiles of the system are presented in Fig. 23 for different time intervals. In the first time interval, from t_1 to t_2 , the battery due to the lower energy cost and amount of power covers the difference between PV generation and load demand. Therefore, the basic operation mode M1 is selected by the EMU. At $t=t_2$, the battery SOC reaches the minimum value (40% as can be seen in the figure) and the battery is not able to supply the load anymore. Therefore, the fuel cell is switched on and continues to cover the energy difference between the PV and load demand and operation mode is changed to M5. At $t=t_3$, the PV generation is more than load demand and therefore fuel cell is turned off. During this time interval, the surplus energy is used to charge the battery when PV generation is less than load demand the difference is supplied by the battery. Therefore, the operation mode at the end of this time interval fluctuates between either M7 or M4 depending on the charging or discharging modes of the battery. The maximum charging and discharging power of the battery needs to be considered and shiftable or dump loads can be used in the case of excessive power generation. It can be seen that during this time interval battery is charged from SOC=40% to SOC=70% although it slightly discharged to SOC=60% at the end. At $t=t_4$, the load demand is more than the PV generation and the difference is more than battery capacity. Therefore, the fuel cell is switched on to supply the difference between the PV generation and the load demand. In this case, the battery is used to compensate for the difference which lets the fuel cell operate with a constant power. The operation mode M5 is selected by EMU. From t_5 to t_6 , the PV power is not available and the load is supplied only by fuel cell and battery. Similar to the previous mode, the fuel cell supplies a constant power to the load and battery compensates for the difference and operation mode is changed to M2. Between t_6 to t_7 , the fuel cell is supplying the load and due to the constant power of

the fuel cell and the command from long-term fuzzy controller, the battery is charged by the fuel cell and the operation mode is changed to M2. The battery should be able to supply the load for the next hours due to the small amount of predicted load demand and long-term energy plan. Therefore, the long-term fuzzy controller increases the desired level of SOC which results in medium and positive values of Δ SOC. Energy distribution and cost analysis of the third energy management scenario are carried out similar to that of the first scenario. As presented in Fig.24, about 54% of the total energy received by the load is provided by the PV, 33% by the fuel cell, and 13 % by the battery. It can be seen that the energy loss in the system is more than that in the grid-connected mode (first scenario). The reason is that in the absence of grid energy, the load energy should be supplied by the renewable energy system and dc-dc converters and inverter. Therefore, increasing power of converters raises the system power loss and consequently energy loss in the micro-grid.

The energy costs of micro-grid in grid-connected and islanded condition with renewable energy sources are compared with the case of using grid only as presented in Fig.25. In the case of grid supply only, the energy cost is calculated based on the time-variable tariffs for grid energy same as the first scenario and the time of energy usage. As can be seen using renewable energy sources along with the grid, reduced the daily energy cost from 2.16 \$/day to 0.66 \$/day. In the case of off-grid condition, the total energy cost is 1.1 \$/day which is about two times of the cost of using grid-connected renewable energy system. Fig.26 shows the total efficiency of the system with and without using SBVB technique. It can be seen that using this technique has reduced the RMS and peak values of current in the windings of the magnetic link and the switching devices and improved the efficiency of the system by almost 4% in 3.5 kW output power. The majority of energy loss in the system attributed to the core loss in the magnetic link as it was fabricated manually in the lab by using thin ribbons of amorphous materials. The micro-grid efficiency can be further improved by using industrial made magnetic cores.

VII. CONCLUSION

Design and development of a fuzzy logic-based energy management unit (EMU) for residential micro-grid applications has been presented. The EMU contained a short-term and a long-term control unit. The long-term controller defined the mandatory changes in the SOC level of the battery and SOH level of hydrogen to meet the long-term energy plans. The short-term controller selected the operation mode of the system based on the real-time values of the energy generation and consumption, energy cost and the required variations of the available capacity of the storage devices. A mode transition unit was designed to smooth the mode changing process using a state transition diagram. To validate the operation of the proposed EMU, a prototype of the system has been developed and experimental tests have been conducted. The operation of the EMU was tested for three different scenarios of the residential load in grid-connected and islanded modes. The energy distribution and energy cost analysis provided for each energy management scenario, showed the benefits of using proposed EMU for both consumer and utility grid.

APPENDIX

Small signal equations and transfer functions of the converters

Bidirectional buck-boost converter	
$\begin{cases} L_1 \frac{di_{L_1}}{dt} = -i_{L_1} r_{L_1} + v_{b2} - v_{C_1} \\ C_2 \frac{dv_{b2}}{dt} = -\frac{v_{b2} - V_{FC}}{R_{FC}} - i_{L_1} - i_o \\ C_1 \frac{dv_{C_1}}{dt} = -\frac{v_{C_1} - V_{BT}}{R_{BT}} + i_{L_1} \end{cases} \quad (12)$	$G_{v-BB}(s) = \frac{\hat{v}_{C_1}(s)}{\hat{d}(s)} = \frac{1}{s + \frac{1}{C_1 R_{BT}}} \cdot \frac{\hat{i}_{L_1}(s)}{\hat{d}(s)} \quad (13)$
$G_{i-BB}(s) = \frac{\hat{i}_{L_1}(s)}{\hat{d}(s)} = \frac{(s + \frac{1}{C_1 R_{BT}}) \left[(s + \frac{1}{C_2 R_{FC}}) \frac{V_{b2}}{L_1} - \frac{D_4 \hat{i}_{L_2}}{L_1 C_2} \right]}{(s + \frac{1}{C_2 R_{FC}})(s + \frac{1}{C_1 R_{BT}})(s + \frac{r_{L_1}}{L_1}) + \frac{(s + \frac{1}{C_2 R_{FC}}) D_4^2 (s + \frac{1}{L_1 C_2})}{L_1 C_1} + \frac{D_4^2 (s + \frac{1}{L_1 C_2})}{L_1 C_2}} \quad (14)$	$H_1(s) = \frac{1}{1 + 0.234s} \quad C_{i-BB}(s) = 2.25 + \frac{0.0018}{s} \quad C_{v-BB}(s) = 0.23 + \frac{15.2}{s} \quad (15) \quad (16) \quad (17)$
Interleaved boost converter	
$\begin{cases} L \frac{di_L}{dt} = V_{PV} - i_L r_L \quad (18) & 0 < t < D_3 T \\ L \frac{di_L}{dt} = V_{PV} - i_L r_L - v_{b3} \quad (19) & D_3 T < t < T \end{cases}$	$\begin{aligned} \text{Current control loop} \quad L \frac{di_L}{dt} &= V_{PV} - i_L r_L - D_3' v_{b3} \quad (20) \\ I_L(s) &= G_{L-V}(s) v_{b3}(s) + G_{L-D}(s) d_3'(s) \quad (21) \\ G_{L-V}(s) &= \frac{-D_3'}{sL + r_L}, \quad G_{L-D}(s) = \frac{-V_{b3}}{sL + r_L} \end{aligned}$
$C_4 \frac{dv_{PV}}{dt} + i_L + \frac{v_{PV}}{R_{mpp}} - I_{mpp} = 0 \quad (22)$	$\text{Voltage control loop} \quad G_{v-PV}(s) = \frac{v_{PV}(s)}{i_L(s)} = \frac{-R_{mpp}}{1 + sC_4 R_{mpp}} \quad (23)$
$H_1(s) = \frac{1}{1 + 0.23s} \quad (24)$	$C_{v-PV}(s) = 0.153 + \frac{14.56}{s} \quad C_{i-PV}(s) = 1.2 + \frac{0.0025}{s} + \frac{2\omega\delta}{s^2 + 4\pi s + (2\omega)^2} \quad (25) \quad (26) \quad (27)$
Control blocks of the TAB converter	
$H_p(s) = \frac{1}{1 + 0.6s} \quad (28)$	$H_c(s) = \frac{1}{C_3 s} \quad C_z(s) = 0.895 + \frac{1.56}{s} \quad C_1(s) = 35 + \frac{185}{s} \quad (29) \quad (30) \quad (31)$

TABLE III
PARAMETERS OF THE MICRO-GRID SYSTEM

Description	Symbol	Value
TAB Converter parameters		
DC voltage of the converter ports	V_{b1}, V_{b2}, V_{b3}	320V, 60V, 110V
Transformer turns ratio	N_1, N_2, N_3	52, 10, 17
Leakage inductances	L_{l1}, L_{l2}, L_{l3}	80 μ H, 5 μ H, 18 μ H
Switching frequency	f_s	10 kHz
DC bus capacitors	C_5	2*470 μ f/400V
Magnetic core shape/dimension	<i>Toroidal</i>	OD=10.5, ID=6.5, W=2.5 (cm)
Magnetic core material	Amorphous	2605SA1
Buck-boost converter parameters		
Fuel cell Emulator	XANTREX-XKW DC P.S.+3*2200 μ f	
Fuel cell Power	P_{FC}	0.8 kW,
Fuel cell voltage/Current	V_{FC}, I_{FC}	30-80 V/10 A
Fuel cell/Battery internal resistance	R_{FC}/R_{BT}	2.5 Ω /0.25 Ω
Fuel cell estimated start-up time	T_{st}	<20s
Battery output capacitor	C_4	420 μ f
Battery/Fuel cell port bus capacitor	C_2	1200 μ f
Battery type	Lead-Acid	4*12 V/100 A.h
Battery Voltage	V_{BT}	24 V
Switching frequency	f_s	10 kHz
Buck-boost inductor	L_1	100 μ H
Interleaved boost converter		
PV power (max)	P_{PV}	1.5kVA
PV Voltage/Current	V_{PV}, I_{PV}	0-30 V/50 A
PV bus capacitor	C_3	1200 μ f
PV Emulator	TDK Lambda300V/11A DC P.S.+ SEMIKRON (SK30GH123) Converter +DSP(TMS28F335)	
PV low pass-filter capacitor	C_1	220 μ f,
Boost inductor	L_2, L_3	80 μ H
Inductor DC resistance	$r_{L1}, r_{L2}/r_{L3}$	0.12 Ω , 0.05 Ω
Bidirectional single-phase inverter		
Inverter output power	P_o	3.5 kW
Output Voltage	V_o	210-250 V
Output low pass filter parameters	L_o, C_o	4mH, 5 μ f/440V ac
AC load power (Max)	P_{LD}	4 kW
Electrolyzer power	P_{EL}	1 kW
Electrolyzer Emulator (Simple Resistor)	R_{EL}	20-50 Ω /1 kW

REFERENCES

- [1] H. Gharavi and R. Ghafurian, "Smart grid: The electric energy system of the future," *Proc. IEEE*, 99(6):917–921, 2011.
- [2] R. Hassan and G. Radman. Survey on smart grid," *IEEE Southeast Con 2010*, pages 210–213, 2010.
- [3] Komminos, N.; Philippou, E.; Pitsillides, A, "Survey in Smart Grid and Smart Home Security: Issues, Challenges and Countermeasures," *IEEE Communications Surveys & Tutorials*, vol.16, no.4, pp.1933,1954, Fourth quarter 2014
- [4] Key World Energy Statistics 2015, <http://www.iea.org/publications>
- [5] Australian PV institute: <http://pv-map.apvi.org.au/historical#4/26.67/134.12>
- [6] Medium term renewable energy market-Report 2015, <http://www.iea.org/bookshop>
- [7] J. Hirsch, "Performance of open-standard PLV technologies on ERDF distribution network," in *Proc. Metering*, London, U.K., Jun. 9–10, 2009.
- [8] H. Kanchev, D. Lu, F. Colas, V. Lazarov and B. Francois, "Energy Management and Operational Planning of a Microgrid With a PV-Based Active Generator for Smart Grid Applications," *IEEE Trans. Ind. Electron.*, vol. 58, no. 10, pp. 4583–4592, Oct. 2011.
- [9] D. Livengood and R. Larson, "The energy box: Locally automated optimal control of residential electricity usage," *Service Science*, vol.1, no. 1, pp. 1–16, 2009.
- [10] N. Navid-Azarbajani, "Load model and control of residential appliances," Ph.D. dissertation, McGill Univ., Montreal, QC, Canada, Aug.1995.
- [11] M. Pedrasa, T. Spooner, and I. Mac Gill, "Scheduling of demand side resources using binary particle swarm optimization," *IEEE Trans. Power Syst.*, vol. 24, no. 3, pp. 1173–1181, Aug. 2009.
- [12] D.-M. Han and J.-H. Lim, "Design and implementation of smart home energy management systems based on zigbee," *IEEE Trans. Consum. Electron.*, vol. 56, no. 3, pp. 1417_1425, Aug. 2010.
- [13] M. Erol-Kantarci and H. T. Mouftah, "Wireless sensor networks for cost-efficient residential energy management in the smart grid," *IEEE Trans. Smart Grid*, vol. 2, no. 2, pp. 314_325, Jun. 2011.
- [14] H. Ghazizai and A. Kadri, "Joint Demand-Side Management in Smart Grid for Green Collaborative Mobile Operators Under Dynamic Pricing and Fairness Setup," *IEEE Trans. Green Communications and Networking*, vol. 1, no. 1, pp. 74-88, March 2017.
- [15] K. Davaslioglu and E. Ayanoglu, "Quantifying Potential Energy Efficiency Gain in Green Cellular Wireless Networks," *IEEE Communications Surveys & Tutorials*, vol. 16, no. 4, pp. 2065-2091, Fourthquarter 2014
- [16] Z. Chen, L. Wu, and Y. Fu, "Real-time price-based demand response management for residential appliances via stochastic optimization and robust optimization," *IEEE Trans. Smart Grid*, vol. 3, no. 4, pp. 1822_1831, Dec. 2012.
- [17] Y. Guo, M. Pan, and Y. Fang, "Optimal power management of residential customers in the smart grid," *IEEE Trans. Parallel Distrib. Syst.*, vol. 23, no. 9, pp. 1593_1606, Sep. 2012
- [18] P. Du and N. Lu, "Appliance commitment for household load scheduling," *IEEE Trans. Smart Grid*, vol. 2, no. 2, pp. 411_419, Jun. 2011.
- [19] R. Palma-Behnke, C. Benavides, F. Lanas, B. Severino, L. Reyes, J. Llanos, and D. Saez, "A microgrid energy management system based on the rolling horizon strategy," *IEEE Trans. Smart Grid*, vol. 4, no. 2, pp. 996–1006, Jun. 2013.
- [20] M. Yazdanian and A. Mehrizi-Sani, "Distributed control techniques in microgrids," *IEEE Trans. Smart Grid*, vol. 5, no. 6, pp. 2901–2909, Nov. 2014
- [21] Q. Jiang, M. Xue, and G. Geng, "Energy management of microgrid in grid-connected and stand-alone modes," *IEEE Trans. Power Syst.*, vol. 28, no. 3, pp. 3380–3389, Aug. 2013.
- [22] R. Miceli, "Energy Management and Smart Grids," *Energies* 2013, 6, 2262-2290.
- [23] E. Muljadi and H. Ed. McKenna, "Power quality issues in a hybrid power system," *IEEE Trans. Ind. Appl.*, vol. 38, no. 3, pp. 803–809, May/June 2002.
- [24] Y. Zhang, A. A. Chowdhury, and D. O. Koval, "Probabilistic wind energy modeling in electric generation system reliability assessment," *IEEE Trans. Ind. Appl.*, vol. 47, no. 3, pp. 1507–1514, May/June 2011.
- [25] M. R. Asghar, G. Dán, D. Miorandi and I. Chlamtac, "Smart Meter Data Privacy: A Survey," *IEEE Communications Surveys & Tutorials*, vol. PP, no. 99, pp. 1-1.
- [26] M. Amer, A. Naaman, N. K. M'Sirdi and A. M. El-Zonkoly, "Smart home energy management systems survey," in *proc. International Conf. Renewable Energies for Developing Countries 2014*, Beirut, 2014, pp. 167-173.
- [27] M. H. Khooban, T. Dragicevic, F. Blaabjerg and M. Delimar, "Shipboard Microgrids: A Novel Approach to Load Frequency Control," *IEEE Trans. on Sustainable Energy*, vol. 9, no. 2, pp. 843-852, April 2018.
- [28] A. A. Ferreira, J. A. Pomilio, G. Spiazzi and L. de Araujo Silva, "Energy Management Fuzzy Logic Supervisory for Electric Vehicle Power Supplies System," *IEEE Trans. Power Electron.*, vol. 23, no. 1, pp. 107-115, Jan. 2008.
- [29] H. Yin, W. Zhou, M. Li, C. Ma and C. Zhao, "An Adaptive Fuzzy Logic-Based Energy Management Strategy on Battery/Ultracapacitor Hybrid Electric Vehicles," *IEEE Trans. Transportation Electrification*, vol. 2, no. 3, pp. 300-311, Sept. 2016.
- [30] D. Arcos-Aviles; J. Pascual; L. Marroyo; P. Sanchis; F. Guinjoan, "Fuzzy Logic-Based Energy Management System Design for Residential Grid-Connected Microgrids," *IEEE Trans. Smart Grid*, vol. PP, no.99, pp.1-1
- [31] S. G. Li, S. Sharkh, F. C. Walsh, and C.-N. Zhang, "Energy and battery management of a plug-in series hybrid electric vehicle using fuzzy logic," *IEEE Trans. Vehic. Tech.*, vol. 60, no. 8, pp. 3571–3585, Oct. 2011.
- [32] Lagorse, J., Simoes, M.G., Miraoui, A., "A multiagent fuzzy-logic-based energy management of hybrid systems," *IEEE Trans. Ind. Appl.*, vol. 45, no. 6, pp. 2123-2129, Nov.-dec. 2009
- [33] L. Igalada, C. Corchero, M. Cruz-Zambrano and F. J. Heredia, "Optimal Energy Management for a Residential Microgrid Including a Vehicle-to-Grid System," *IEEE Trans. Smart Grid*, vol. 5, no. 4, pp. 2163-2172, July 2014.
- [34] S. Falcones, R. Ayyanar and X. Mao, "A DC–DC Multiport-Converter-Based Solid-State Transformer Integrating Distributed Generation and Storage," *IEEE Trans. Power Electron.*, vol. 28, no. 5, pp. 2192-2203, May 2013.
- [35] H. Tao, A. Kotsopoulos, J. L. Duarte and M. A. M. Hendrix, "Transformer-Coupled Multiport ZVS Bidirectional DC–DC Converter With Wide Input Range," *IEEE Trans. Power Electron.*, vol. 23, no. 2, pp. 771-781, March 2008.
- [36] Tao, H.(2008).Phd thesis, Integration of sustainable energy sources through power electronic converters in small distributed electricity generation systems Eindhoven: Technische Universiteit Eindhoven DOI: 10.6100/IR632347
- [37] D. Liu and H. Li, "A ZVS Bi-Directional DC-DC Converter for Multiple Energy Storage Elements," *IEEE Trans. Power Electron.*, vol. 21, no. 5, pp. 1513-1517, Sept. 2006.
- [38] M. Phattanasak, R. Gavagsaz-Ghoachani, J. P. Martin, B. Nahid-Mobarakeh, S. Pierfederici and B. Davat, "Control of a Hybrid Energy Source Comprising a Fuel Cell and Two Storage Devices Using Isolated Three-Port Bidirectional DC–DC Converters," *IEEE Trans. Ind. Appl.*, vol. 51, no. 1, pp. 491-497, Jan.-Feb. 2015.
- [39] R. W. A. A. De Doncker, D. M. Divan and M. H. Kheraluwala, "A three-phase soft-switched high-power-density DC/DC converter for high-power applications," *IEEE Trans. Ind. Appl.*, vol. 27, no. 1, pp. 63-73, Jan/Feb 1991.
- [40] M. Rakhshan, N. Vafamand, M. H. Khooban and F. Blaabjerg, "Maximum Power Point Tracking Control of Photovoltaic Systems: A Polynomial Fuzzy Model-Based Approach," *IEEE Journal of Emerging and Selected Topics in Power Electronics*, vol. 6, no. 1, pp. 292-299, March 2018.
- [41] R. Zhang and J. Tao, "GA based fuzzy energy management system for FC/SC powered HEV considering H2 consumption and load variation," *IEEE Trans. on Fuzzy Systems*.
- [42] S. Njoya Motapon, L. A. Dessaint and K. Al-Haddad, "A Comparative Study of Energy Management Schemes for a Fuel-Cell Hybrid Emergency Power System of More-Electric Aircraft," *IEEE Trans. on Ind. Electronics*, vol. 61, no. 3, pp. 1320-1334, March 2014.
- [43] <http://www.cleanenergyregulator.gov.au/RET/Scheme-participants-and-industry/Agents-and-installers/Installation-requirements-for-small-scale-systems>
- [44] <https://standards.ieee.org/findstds/standard/1547-2018.html>

- [45] Y. Shi, R. Li, Y. Xue and H. Li, "High-Frequency-Link-Based Grid-Tied PV System With Small DC-Link Capacitor and Low-Frequency Ripple-Free Maximum Power Point Tracking," *IEEE Trans. Power Electron.* vol. 31, no. 1, pp. 328-339, Jan. 2016.
- [46] F. Liu, S. Duan, F. Liu, B. Liu and Y. Kang, "A Variable Step Size INC MPPT Method for PV Systems," *IEEE Trans. Ind. Electron.*, vol. 55, no. 7, pp. 2622-2628, July 2008
- [47] C.L.Phillips and H.T.Nagle, "Digital control systems analysis and design," 3rd edition, New Jersey, USA, *Prentice-Hall*, 1995.
- [48] O. Hegazy, J. V. Mierlo and P. Lataire, "Analysis, Modeling, and Implementation of a Multidevice Interleaved DC/DC Converter for Fuel Cell Hybrid Electric Vehicles," *IEEE Trans. Power Electron.*, vol. 27, no. 11, pp. 4445-4458, Nov. 2012.
- [49] A. Karimi, D. Garcia and R. Longchamp, "PID controller tuning using Bode's integrals," *IEEE Trans. Control Systems Technology*, vol. 11, no. 6, pp. 812-821, Nov. 2003
- [50] B. Yang, W. Li, Y. Zhao and X. He, "Design and Analysis of a Grid-Connected Photovoltaic Power System," *IEEE Trans. Power Electron.*, vol. 25, no. 4, pp. 992-1000, April 2010
- [51] Y. Sun, X. Hou, J. Yang, H. Han, M. Su and J. M. Guerrero, "New Perspectives on Droop Control in AC Microgrid," *IEEE Trans. Ind. Electron.*, vol. 64, no. 7, pp. 5741-5745, July 2017.
- [52] <https://www.horizonfuelcell.com/h-series-stacks>



Jianguo Zhu (S'93–M'96–SM'03) received the B.E. degree in 1982 from Jiangsu Institute of Technology, Jiangsu, China, the M.E. degree in 1987 from Shanghai University of Technology, Shanghai, China, and the Ph.D. degree in 1995 from the University of Technology Sydney (UTS), Sydney, Australia, all in electrical engineering. He was appointed a lecturer at UTS in 1994 and promoted to full professor in 2004 and Distinguished Professor of Electrical Engineering in 2017. In 2018, he joined the University of Sydney, Australia, as a full professor and Head of School, School of Electrical and Information Engineering. His research interests include computational electromagnetics, measurement and modelling of magnetic properties of materials, electrical machines and drives, power electronics, renewable energy systems and smart micro grids.



Mohammad Jafari (M'12) received the B.E. degree from Shiraz University, Shiraz, Iran, in 1998, the M.E. degree from Guilan University, Rasht, Iran, in 2001 and, the Ph.D. degree from University of Technology Sydney (UTS), Sydney, Australia, in 2017 all in electrical engineering. From 2001 to 2011, he contributed to the design and development of many industrial power electronic projects. Since 2012, he has been with the UTS as a lecturer. His

current research interests include power electronic converters and drives, renewable energy systems and smart micro-grids.



Zahra Malekjamshidi (S'13) received the B.E. and M.E. degrees from Shiraz University, Shiraz, Iran, in 1998, and 2001 respectively, both in electrical engineering. She is currently working toward the Ph.D. degree at the University of Technology Sydney (UTS), Sydney, Australia. From 2002 to 2012, she worked as a research engineer and contributed to the design and development power electronic projects. Her current research interests include

matrix converters, dc-dc converters, renewable energy technologies and smart micro-grids.



Dylan Dah-Chuan Lu received his B.E. and Ph.D. degrees from The Hong Kong Polytechnic University, Hong Kong, in 1999 and 2004 respectively. In 2003, he joined PowerLab Ltd. as a Senior Design Engineer and was responsible for industrial switching power supply projects. He was a full-time faculty member with The University of Sydney from 2006 to 2016. He now holds an Honorary position at the University of Sydney. Since July 2016, he has been an Associate Professor at the School of Electrical and Data Engineering,

University of Technology Sydney, Australia. His current research interest includes efficient and reliable power conversion for renewable sources, energy storage systems, and microgrids. He is a senior member of IEEE and a member of Engineers Australia. He was the recipient of the Best Paper Award in the category of Emerging Power Electronic Technique at the *IEEE PEDS* 2015. He presently serves as an Associate Editor of the *IEEE Transactions on Circuits and Systems II* and a Subject Editor of the *IET Renewable Power Generation*.